EMISSION CHARACTERISTICS OF A SOLUTION PROCESSED, SINGLE LAYER WHITE ORGANIC LIGHT EMITTING DIODE

A Thesis Submitted to
the Graduate School of
İzmir Institute of Technology
in Partial Fulfillment of the Requirements for the Degree of

MASTER OF SCIENCE

in Photonics Science and Engineering

by
Volkan BOZKUŞ

December 2020
İZMİR

ACKNOWLEDGMENTS

ABSTRACT

EMISSION CHARACTERISTICS OF A SOLUTION PROCESSED, SINGLE LAYER WHITE ORGANIC LIGHT EMITTING DIODE

White organic light emitting diodes (WOLEDs) are getting more attention day by day because of their some superior properties like viewing angle, refresh rate, flexibility, easy production process and consequently relatively cost-effective natures. Within the scope of this thesis, WOLED has been prepared and characterized by using the single emitter layer prepared by solution process method. In the emission layer, the host material is used for both obtaining the blue region of the visible spectrum and for efficient energy transfer to the green and orange-red guest material. Poly(N-vinylcarbazole) (PVK): 2-(4-Biphenylyl)-5-phenyl-1,3,4-oxadiazole (PBD) or 1,3-bis[(4-tert-butylphenyl)-1,3,4-oxadiazolyl] phenylene (OXD-7) matrices are used as host for orange-red emitting material of N,N'-bis(2-ethylhexyl)perylene-3,4,9,10-dicarboxylic diimide (PDI) and green emitting material of perylene-3,4,9,10-tetracarboxy tetrabutylester (PTE).

Electron and hole mobility, L-V-J characteristics and morphologies of two different host matrix of PVK:PBD and PVK:OXD-7 were examined. As a result of these evaluations, the appropriate host was determined as PVK:PBD. Host:PTE and Host:PDI emission characteristics were examined and exciplex, electroplex formations were detected. After, Host:PTE:PDI configuration were discussed and high white light properties of optimized WOLED are displayed CIE 1931 coordinates (x, y) of (0.34, 0.36), correlated colour temperature of 4916 K and CRI of 96. Finally, lethal time 70 of the latest devices was examined.

ÖZET

ÇÖZELTİ SÜREÇLİ, TEK TABAKA BİR BEYAZ IŞIK YAYAN ORGANİK DİYOTUN EMİSYON ÖZELLİKLERİ

Beyaz ışık yayan Organik Diyotlar (WOLED'ler) geniş görüş açısı, yüksek yenileme hızı, esneklik, kolay üretimi ve uygun maliyetleri gibi üstün özellikleri nedeniyle gün geçtikçe daha çok ilgi çekmektedirler. Bu tez kapsamında çözelti süreçli, tek ışıma tabakası kullanılarak WOLED hazırlanmış ve ışıma katmanında bulunan konak malzemesi hem mavi ışıma hem de konuk malzemesine enerji transferini için kullanılmıştır. Poly(N-vinylcarbazole)(PVK): 2-(4-Biphenylyl)-5-phenyl-1,3,4 oxadiazole (PBD) veya 1,3-bis[(4-tert-butylphenyl)-1,3,4-oxadiazolyl] phenylene (OXD-7) matrisleri, turuncu-kırmızı ışıma yapan N,N'-bis(2-ethylhexyl)perylene-3,4,9,10-dicarboxylic diimide (PDI) ve yeşil ışıma yapan perylene-3,4,9,10-tetracarboxy tetrabutylester (PTE) perilen türevleri için konak olarak kullanılmıştır.

İki farklı konak matrisi olan PVK:PBD ve PVK:OXD-7'ye ait elektron ve boşluk hareketliliği, akım yoğunluğu-gerilim-ışıma karakterleri ve morfolojik incelemeleri yapıldı. Bu incelemeler sonucunda PVK:PBD uygun konak olarak tespit edildi ve devamında PTE ve PDI:PTE katkılama oranları belirlendi. Konak olan PVK:PBD matrisine PTE katkınlaması durumunda eksipleks, PDI katkınlaması durumunda ise elektropleks oluşumları tespit edildi. Daha sonra, konak:PTE:PDI konfigürasyonu incelendi ve optimize edilen WOLED, (0.34, 0.36) CIE 1931(x, y) koordinatları, 4916 K renk sıcaklığı ve 96 renksel geriverim indeksi (CRI) elde edildi. Son olarak optimize edilen aygıtların yaşam ömürleri incelendi.

To my family…

TABLE OF CONTENTS

LIST OF FIGURES

LIST OF TABLES

LIST OF SYMBOLS AND ABBREVIATIONS

AFM	Atomic Force Microscopy
CCT	Correlated Colour Temperature
CIE	Commission Internationale de l'éclairage
CRI	Colour Rendering Index
EIL	Electron Injection Layer
EL	Electroluminance
EML	Emissive layer
FRET	Förster Resonance Electron Transfer
HCl	Hydrochloric acid
HOMO	Highest Occupied Molecular Orbital
ITO	Indium tin oxide
LCD	Liquid-Crystal Display
LiF	Lithium fluoride
LUMO	Lowest Unoccupied Molecular Orbital
OFET	Organic Field Effect Transistor
OLED	Organic Light Emitting Diode
OXD-7	1,3-bis[(4-tert-butylphenyl)-1,3,4-oxadiazolyl]phenylene
PBD	2-(4-Biphenylyl)-5-phenyl-1,3,4-oxadiazole
PDI	N,N'-bis(2-ethylhexyl)perylene-3,4,9,10-dicarboxylic diimide
PEDOT:PSS	Poly(3,4-ethylenedioxythiophene):poly(styrene sulfonate)
PL	Photoluminescence
PTE	Perylene-3,4,9,10-tetracarboxy tetrabutylester
PVD	Physical Vapor Deposition
PVK	Poly (N-vinylcarbazole)
SCLC	Space charge limited current
TPQ	Triplet exciton-Polaron quenching
TTA	Triplet-Triplet Annihilation
UV-Vis	Ultraviolet-visible
WOLED	White Organic Light Emitting Diode
Å	Angstrom
Al	Aluminium

Au	Gold
ε	Electrical permittivity of material
ε_0	Electrical permittivity of free space
k_q	rate constant
LT70	Lethal Time 70
$L–V–J$	Luminance–Voltage–Current density
M	Molarity
nm	Nanometre
PS	Polystyrene
Q	Concentration
rms	root mean square
wt	Ultraviolet
λ	Wavelength
λ_{ext}	Excitation wavelength
τ_0	Life time

CHAPTER 1

INTRODUCTION

Being able to perceive light is the most effective way to recognize and react to environment. Scientists who have understood the importance of light throughout history have started to think and research about the fundamentals of light. One of the earliest known examples of the behaviour of light discovered in history belongs to the Chinese philosopher Mo-ti. He discovered camera obscura after named pinhole camera claiming that light moves linearly and reflected backwards on the screen after passing through a small hole [1]. Many scientists have worked to understand nature of light like Aristotle, Ibn al-Haytham, Newton, Christiaan Huyghens, Albert Einstein and many more. Each tried to understand the nature of light and explained it with known laws. As an example, the most famous of these has been whether the light is a particle or a wave. At this point, according to experimental setup, it was seen that light behaved like particles and sometimes waves. This showed that particle and wave properties of light coexist in the form of duality which can only reveal one depends on experiment [2].
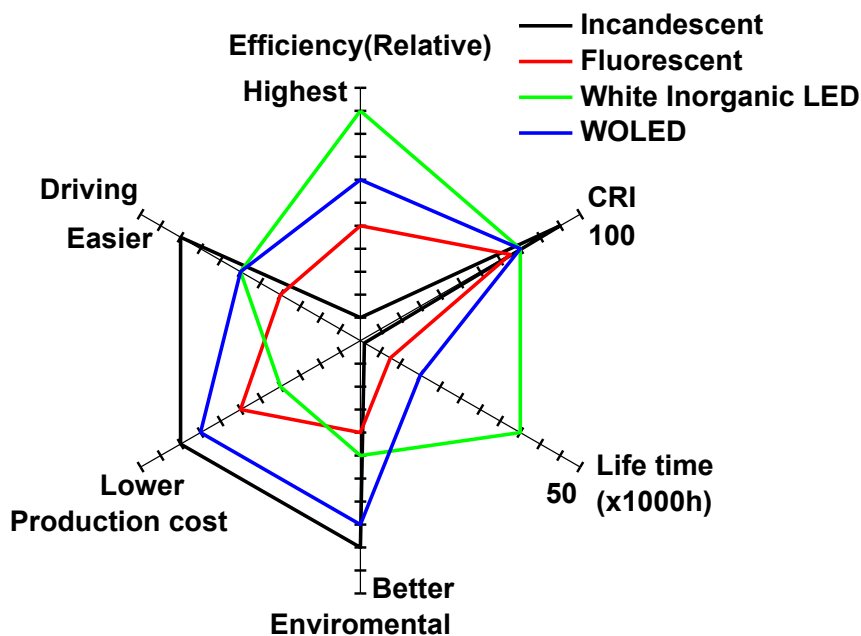
Figure 1.1 Comparison of efficiency, lifetime, environment, CRI, driving and production const, which are important parameters for lighting devices (adapted from [3] and updated from [4]).

Understanding the nature of light that is vital for life has increased methods of obtaining it and its usage areas. While in the earlier times, light requirement obtained by sun and fire, different methods have been developed later. Edison invented a useful incandescent lamp for the first-time using electricity with the help of a tungsten filament. However, instead of these inefficient methods, later fluorescent lamps and nowadays solid-state lighting devices have been developed. Advantages and disadvantages of these lighting methods compared to each other are summarized in figure 1.1. In general, incandescent and OLEDs are advantageous in terms of easy production, usability, light quality and environmental friendliness, while inorganic LED is advantageous in terms of efficiency and lifetime.

Organic light emitting diodes (OLEDs) have rapid increase as one of the technologies for display screens and solid-state lightning technology due to their outstanding features. Compared to LCD technology, LCD still dominates current market but has some limitations such as resolution, refresh rate and colour quality. Furthermore, OLED displays do not need backlighting, so they are not heavy and have a wide viewing angle.

Figure 1.2 LG WX 65 inch Class Wallpaper 4K Smart OLED TV w/ AI ThinQ [5]

Although efficiency and life span are still challenge, it has started to be used commercially in lighting and display technologies (Phillips, LG, Samsung etc.) overcoming this problem by inventive methods. OLEDs are pioneers in titles such as design, innovation, flexibility and slimness. An OLED with a thickness of 0.3 mm was produced in a study by Brian W. D'Andrade et al. According to the result of this study,

which was developed as a prototype, such OLEDs can be easily transported and mounted directly on the wall [6]. Figure 1.2 shows a commercially produced OLED TV by LG and only has 3.81 mm thin display. The success of obtained white light depends on energy levels of the visible wavelength range of the solar spectrum simulated by the use of appropriate semiconductors. The minimum requirement for white light is the combination of red-orange and blue colours. However, in order to obtain high quality white light, at least blue, green and red emission need be combining.

1.1. White Light Quality Parameters

Some definitions have been created in order to quantify the quality of white light. Color rendering index (CRI) color correlated temperature (CCT) and CIE 1931 (Commission Internationale d'Eclairage) is the important parameter in the classification of light, especially white light.

CIE coordinates were developed in 1931 by International Commission on Illumination (Commission Internationale d'Eclairage ,CIE) to characterize the colour of light emitted from any source [7]. The X, Y and Z tristimulus values formulated as follows, are basically based on three types of color sensitive cones found in the human eye, which enable the perception of colors.

$$X = \int_\lambda \bar{x}\ (\lambda)P(\lambda)d\lambda \qquad\qquad 1.1$$

$$Y = \int_\lambda \bar{y}\ (\lambda)P(\lambda)d\lambda \qquad\qquad 1.2$$

$$Z = \int_\lambda \bar{z}\ (\lambda)P(\lambda)d\lambda \qquad\qquad 1.3$$

Where λ is wavelength in the range of 380 to 780 unit of nanometer. $\bar{x}(\lambda)$, $\bar{y}(\lambda)$ and $\bar{z}(\lambda)$ values are the human eye colour sensitivity and $P(\lambda)$ is the spectral radiance of source. Chromaticity coordinates can be found as fallows;

$$x = \frac{X}{X+Y+Z} \qquad\qquad 1.4$$

$$y = \frac{Y}{X+Y+Z} \qquad\qquad 1.5$$

$$z = \frac{Z}{X+Y+Z} \qquad\qquad 1.6$$

Since z= 1-x-y, colour coordinates can only be represented in terms of x and y. For ideal white light, the x and y coordinates are defined as 0.33, 0.33. However, it also exhibits white light characteristics in a large area around this region.

The colour rendering index (CRI) is a quantitative measure, which compares the colour of an object illuminated by a source with the colour of an object illuminated by natural or ideal sources. The CRI value of a light source is determined by comparing reflections from 8 different colour standard samples illuminated by both the light source and the black body with the same colour temperature. The CRI value varies between 0 and 100. It is desirable to have a high CRI value. High CRI value means that objects reflect their true colours. Another method used to characterize light is colour correlated temperature (CCT) value. CCT value is determined by comparing the light coming from a source with the black body radiator. There is a fundamental difference between CCT and CRI values. Although two light sources with the same CIE coordinates and same CCT value, the colours of an object illuminated by these sources may be perceived differently. This difference is understood with the definition of CRI [8].

1.2. Background of White Organic Light Emitting Diodes

With the understanding of semiconductor physics, the first light emitting diodes (LEDs) were reported by O.V. Lossev in 1927 [9]. Although an efficient LED could not be obtained in this first study, it attracted the attention of many researchers. LED studies continue today, but the search for light sources is not limited to LEDs. After the artificial lights started to be obtained efficiently, the light quality started to be emphasized. Light emitting diodes made with organic materials are important in this regard. First study on organic light emitting diodes (OLEDs) made by Pope et al in 1963 by the use of anthracene film between electrodes. This study is important for being the first, but it can operate under very high potential about 100V [10]. In 1987, Tang and his colleagues obtained the first efficient OLED in Eastman Kodak Company by using materials that transmit electrons and holes separately electrodes resulted low voltage operation. This study, recognized as the first OLED for many, was created using bilayer method coating tris(8-hydroxyquinoline)aluminum (Alq3) and diamine materials in the form of thin layer between the electrodes [11]. Later, many researchers in the field of OLED used different methods and materials that provided development of this technology.

First white light emitting OLED, shortly white organic light emitting diode (WOLED), was obtained in 1994 by Kido et al [12]. After this invention, significant progress has been made in both academic and industrial areas in terms of efficient OLED lighting. In this study, orange, green and blue fluorescent materials were added to poly

(N-vinylcarbazole) material, which is a hole transfer material. This WOLED with an efficiency factor of 1 lm/W is very successful in terms of being the first example. WOLED studies by Adamovich et al, the power efficiency(Lm/W) reached the level of tungsten filament lamps of 10 lm/W for the first time [13]. High refractive indexes of organic materials, optical confinement, total internal reflection causes low efficiency in organic light emitting diodes. In a study by Sun et al., about 70 lm/W was reached by making using low index grid and optical optimizations [14]. Another WOLED studies by Sebastian Reineke et al, in 2009 [15], are important in terms of reaching above 90 lm/W, which is the power efficiency of standard fluorescent lamps. Some of the light generated in the active layer cannot go out due to light out coupling. The work is also an important factor for light out coupling enhancement. The refractive index of glass is 1.5, while organic materials are around 1.8. Different refractive index cause total internal reflection determined by Snell law. By keeping the refractive index of the substrate and organic materials close to each other, total internal reflection is prevented Another method to reduce the total internal reflection rate is to keep the angle of incidence of the light perpendicular to the substrate surface. Making the substrate hemispherical made it possible to keep the angle close to perpendicular in all directions. They achieved a maximum power efficiency of 124 lm /W and they compromised the quality of white light and stated that high CRI can be achieved in case of light out coupling enhancement.

OSRAM company took the first step in the commercialization of WOLEDs and in 2008. They introduced a hybrid lamp (PirOLED) in which WOLED and LEDs are used together. Output of the OLLA project was a breakthrough in obtaining white light from devices made using organic materials [16]. In the following years, developments in the field of WOLED continued and both efficiency and light quality were improved. White light emitting organic diodes (WOLED) are defined as new generation energy efficient lighting devices. For this reason, in recent years, many projects have been carried out on WOLEDs supported by the EU and many countries For example, important projects such as OLLA, a European Union project that ended in 2008, and OLED100.eu, a follow-up study, have been carried out The OLED100.eu project, which cost 30 million dollars (20 million dollars by EU) was supported by companies such as Philips, OSRAM, Siemens, Novaled, Franhofer IPMS. Another EU project named CombOLED lead by OSRAM was created to develop low-cost and innovative device architectures using less complex materials [17,18]. The SOLEDLIGHT project has been supported in 2015 by EU to obtain at least 100 lm/W cost efficient light by roll-to roll (R2R) solution processed method [19]. The first output of

this project was published in 2016 by Aghazada et al. In this work [20], HIL, HTL and EML coated by spin coating method then ETL and cathode coated with PVD reached 6.3 lm/W.
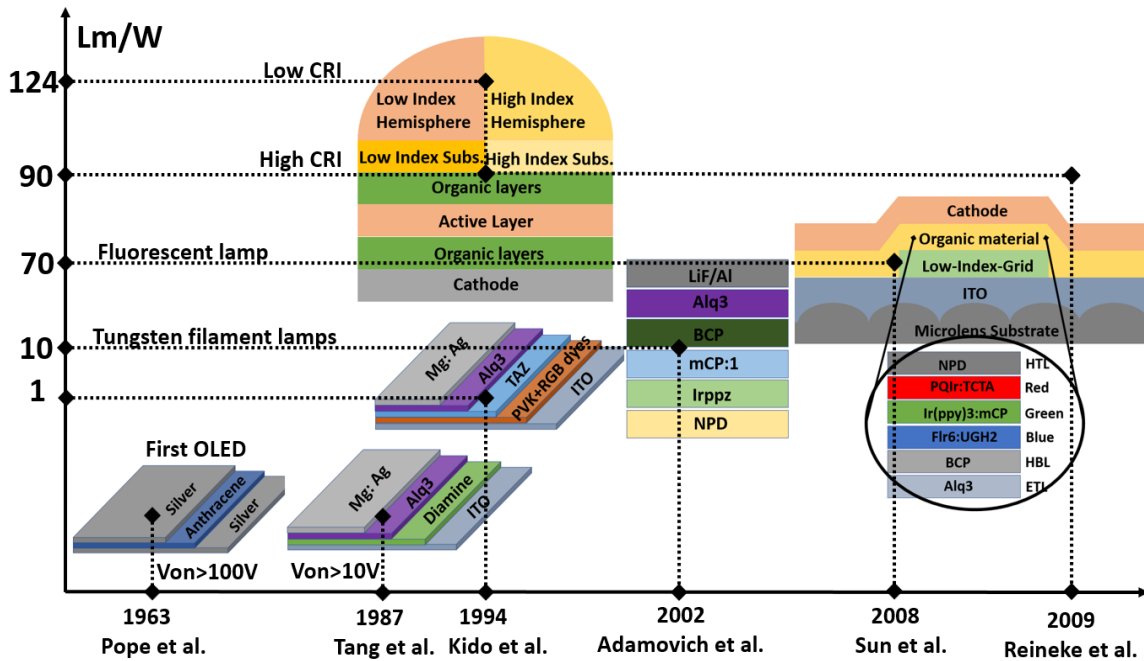
Figure 1.3 WOLED development over the years

1.3. Device Architectures and Coating Techniques Employed

Organic light emitting diodes (OLEDs), as the simplest definition, are devices with a sandwich structure obtained by coating organic materials as thin films between two electrodes. OLEDs structures formed by combining electrons and holes transferred from the cathode and anode in the emissive layer (EML). Extra layers can be used for efficient transfer of charges. Working principle of an OLED in energy dimension is given in figure 1.4. There are different approaches such as the number of layers, the coating method, the outflow direction of the light, electrical feeding. White light obtained in the vertically stacked structure (figure 1.5a) WOLED approach originates from feeding each emission layer separately. In vertically stacked structures, white light is produced by OLEDs connected in series. In this structure there is charge generation layer between each them. In this way, the voltage needed for each structure can be applied and this allows it to operate at low voltage. The most important disadvantage is the difficulty of fabricating these structures. However, it is very difficult to produce WOLED with this method. Since each layer is fed separately, electrical supply and optimization is easier. On the other

6

hand, optical cavity still remains a problem. The light created in the active layer has to pass through other layers in order to get out Especially considering that white light consists of different colours and that each colour must face with different refractive index, it is understood that optimizing will remain a problem [21–23].
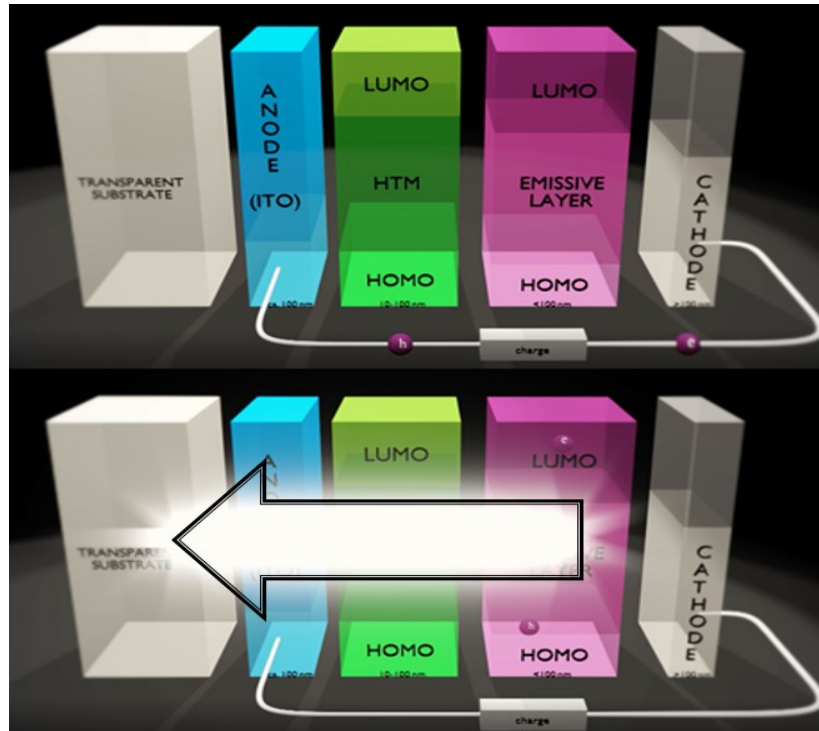
Figure 1.4 Fundamental working principle of OLED

Since white light is basically a combination of three primary colours, a balance of these colours must be achieved in order to obtain high quality white light. The desired balance of colours can only be possible with charge and exciton manipulation. Multi-EML (figure 1.5b) method provides a great advantage in this respect. Deficit of this method is that it is relatively difficult to manufacture and inconvenient for wet coating methods. Morphological disturbances between layers in wet coating methods make optimization in the device difficult. PVD technique has to be used widely, which is a factor that increases the cost [24–26].

Devices prepared by obtaining single-EML (figure 1.5c) were the most effective due to low production cost and simple device structure. To obtain white light in a single layer, molecules with different emission regions must coexist in the active layer. At least complementary (blue and orange-red) or primary (blue, green and red) colours must be use together for white light generation. WOLED made by Alam et al. by using two different polymers, which is poli(9,9-dioktilfluoren) (PFO) and poli[2-metoksi-5-(2'-etil-

7

hekzilokzi)-1,4-fenilenvinilen] (MEH-PPV). As a result of incomplete energy transfer from PFO to MEH-PPV, white light was obtained from mixture of two polymers [27]. Single emitter device structure is cost effective method also allows to enlarge the area because of easy to apply but have back draw in manipulating exciton formation.
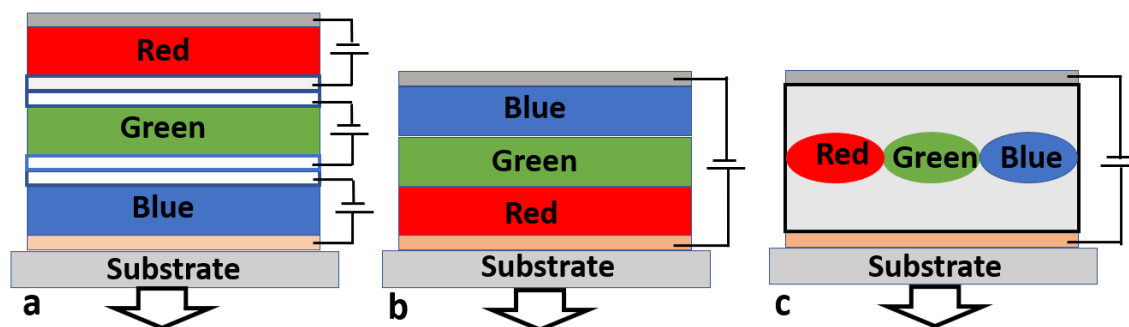
Figure 1.5 Fundamental OLED fabrication structure a) vertically stacked b) multi-EML c) single-EML[28]

To summarize, soluble materials are generally coated by wet coating, and insoluble materials by thermal evaporation. Polymeric structures are generally soluble and small molecules are generally insoluble. However, there are also polymers and small molecules that do not conform to this generalization.

There is more than one method in preparation of thin films, which should generally be thinner than 100nm. Each coating method has some advantages and disadvantages. Basically, the coating method is divided into two: the first is the solution process (or wet process) and the second is the physical vapor deposition. In solution process, material to be coated is dissolved or dispersed in a solvent then this solution phase is applied on substrate and solvent is evaporated. There are several methods to apply the solution phase as a thin film, these are spin coating, doctor blade, dip coating, inkjet printing, spray. In all of these, the film thickness can be partially controlled. The thickness of the film formed in the solution phase mostly depends on the concentration. There are other parameters that affect the film thickness thanks to the coating method. For example, rotation speed (angular velocity) affects the film thickness in the spin coating method, while the drawing speed (linear velocity) from the solvent affects in the dip coating method. Wet coating methods have the potential to reduce costs by preventing material waste, faster. However, there are some problems with the wet coating method to solve. The biggest problem is encountered in multilayer coating. Film coated in solution

process may damage the underlying film can causes uncontrollable optical and electrical problems.

In the physical vapor deposition (PVD) method, organic materials are evaporated under high pressure (10^{-6} mbar) and coated on the substrate. Thickness of film can be controlled sensitively considering the evaporation temperature of the material. Although it allows the fabrication of multilayer structures, materials with low degradation temperatures are not suitable for this type of coating technique.

1.4. Organic Semiconductors

Alan J. Hegeer, Alan G. MacDiarmid and Hideki Shirakawa, who discovered conductive polymers by doping halogen and received Nobel prize in 2000 for chemistry. Thus, polymers have begun to be used and researched more widely in the field of electronics, their being synthesizable and easy to use in solution phase have been the biggest advantages. Organic materials began to be used in the field of OLEDs, OFETs, sensors, organic photovoltaics after the discovery of these properties. The materials used in the field of organic electronics are generally conjugated molecules. Carbons conjugated with strong covalent bonds generates sp^2 hybrid orbital with σ bond and p_z orbital. When organic molecules are very close to each other, p_z orbitals overlaps thus π bonds are formed. These π bonds formed are delocalized on the molecule, which provides conductivity [29,30].
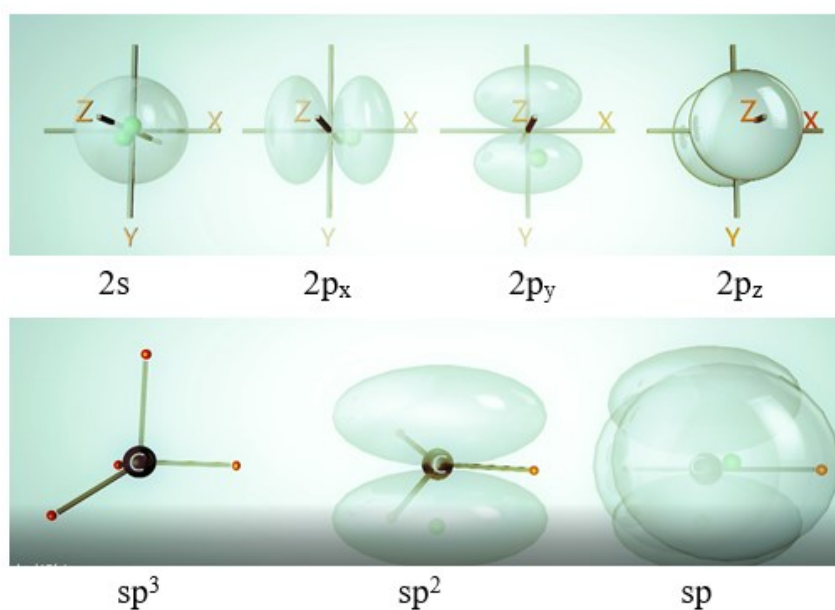
Figure 1.6 Schematic illustration of orbitals

Structures similar to valance and conduction bands in inorganic materials are also seen in organic materials. The combination of pi orbitals can form degenerate stats. In such a case, energy levels may (filled or unfilled bonds) occur at the same level or very close to each other, or in places where energy levels are not exist. Unlike inorganic materials, these levels are called molecular orbitals. For radiative transition there must be a transition between the highest occupied molecular orbital (HOMO) and lowest unoccupied molecular orbital (LUMO) (Figure 1.4).

The Jablonski Diagram, named after physicist Aleksander Jabloński, best summarizes the energy levels in organic molecules and the possible transitions between these levels. Provides information on absorption fluorescence phosphorescence and delayed fluorescence transitions and other non-radiative transitions. If light with higher energy than the band gap of the semiconductor is sent onto the semiconductor, this light can be absorbed. Transfer process of the electron in the excited state and the type of radiation can be defined by this diagram.
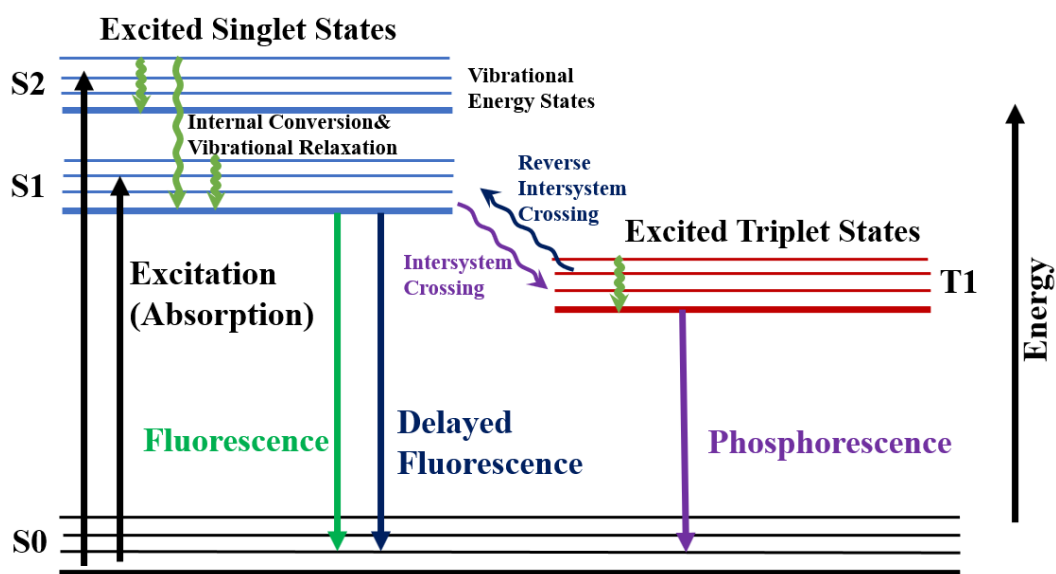
Figure 1.7 Energy and electron transfer processes illustrated by the Jablonski diagram

For fundamentals of spin-statistic fluorescent is less efficient then phosphorescent and TADF materials. The reason is that the quantum mechanically formed singlet triplet energy levels have different rates of exciton. electrically injected singlets and triplets are formed in a ratio of 1:3 so the singlet emitting material can only use 25 percent of the injected charges as radiative recombination [31,32]. Phosphorescent and TADF emitter materials use rare heavy metals such as platinum or iridium to enable a quantum-

mechanical phenomenon called spin-orbit coupling, which increases the radiative rate of triplet excitons. It is not only expensive due to the heavy metals it contains, but also causes environmental pollution and toxicity. In the preparation of WOLED, the use of materials showing phosphorescent properties is quite common. However, the use of phosphorescent materials in OLEDs brings new problems. Triplet exciton-polaron (TPQ) and triplet-triplet annihilation (TTA) are likely to occur due to the high life time (10^{-6}-10^{-3}s) of triplet excitons [33]. Additionally, the high triplet exciton diffusion length (<100 nm) makes the device architecture difficult to control and increases the probability of energy losses. The long-life time of excitons increases the exciton density in the active layer and increases the possibility of excitons to interaction. These negativities cause a decrease in efficiency and therefore a decrease in strength with the increase of brightness. Since the life time (10^{-9}s) and diffusion length (<20nm) of singlet excitons are lower than the triplet exciton, such an effect is not encountered. The main problem is encountered in white light generation. While TTA and TPQ occurs in the active layer, the wavelength does not remain constant and shifts occur. In such a situation, the increase in voltage will exacerbate this shift. As a result, they create problems in CRI, CCT and CIE issues in white light production [34–38]. Another fact is that OLEDs using blue phosphorescent materials have a very low lifespan and it is very difficult to obtain WOLEDs with high CRI values due to the fact that the radiation of blue phosphorescent materials is closer to the green region [39].

Actually, not only the efficiency but also the pace of radiative recombination zone highly dependent on the electron and hole balance. In order to achieve this balance, it is very important to know the electron and hole mobility, and to design the materials and device accordingly. Mobility define how fast an electron drifts under an electric field. There are many ways to find the mobility of a semiconductor such as hall effect, field effect transistor, and space charge limited current [40,41]. SCLC method well established and easy. Current density can be examined in four sections. These can be listed as ohmic zone (J_{OHM}), space charge limited zone (J_{SCL}), trap charge limited zone (J_{TCL}), trap charge filled zone (J_{TFL}). Current density at low voltage is determined by the ohm's law as follows;

$$J_{OHM} = eN_0\mu\frac{V}{d} \qquad\qquad 1.7$$

where V is voltage, N_0 is free electron per unit surface, e is electron charge, μ is mobility and d indicates the thickness between electrodes. When the voltage starts to increase, the

charges begin to accumulate in the active area and after a certain voltage, these charges begin to flow in proportion to the square of the applied voltage. This regime called as SCLC. When voltage is applied to the electrodes, the charged particle between the electrodes moves as follows;

$$v = \mu E \qquad\qquad 1.8$$

where v is speed of charges E is electric field. Similarly, the representation of current density depending on conductivity (σ) is as follows;

$$J = \sigma E \qquad\qquad 1.9$$

The equation connecting the electron (n) and hole (p) density as a function of one direction to the conductivity is as follows;

$$\sigma = en(x)\mu_e + ep(x)\mu_p \qquad\qquad 1.10$$

where μ_e and μ_p is electron and hole mobility, respectively. If we combine this equation with equation 1.3;

$$J = en(x)\mu_e E + ep(x)\mu_p E \qquad\qquad 1.11$$

If we rearrange all these with the electric field in the insulator with the Poisson equation, we have;

$$\frac{dE}{dx} = \frac{en(x)}{\varepsilon} \qquad , \frac{dE}{dx} = \frac{ep(x)}{\varepsilon} \qquad\qquad 1.12$$

Solving these equations under V (0) = V and V (L) = 0 boundary condition, will result;

$$J_{SCLC} = \frac{9}{8}\varepsilon\varepsilon_0\,\mu\frac{V^2}{d^3} \qquad\qquad 1.13$$

where ε and ε_0 is the permittivity of material and free space, respectively. Mobility can be found by making electron only and hole only devices. To find the permittivity of the material between electrodes, which are parallel plates, it is necessary to measure its capacitance.

1.5. WOLEDs Based on Perylene Derivatives

Perylene diimides (PDIs) attract attention due to their superior properties such as high thermal, optical and chemical stability, very high molar absorption coefficients (10^4 $M^{-1}cm^{-1}$) in the visible region, fluorescence quantum yields of 90% in the solution phase high electron affinities, electron mobility and relatively easy to chemical modifications [42–44]. Excited-state electrons do not transition from singlet to triplet and absorbed energy

transforms from singlet to fluorescence with little loss and absorbed energy transforms into fluorescent emission with minor loss [45]. However, besides all these positive properties, it tends to aggregate in the film phase as a result of strong π-π interactions in the perylene core. Micrometer sized crystallites formed as a result of aggregation cause aggregation damping and decrease in fluorescence quantum yields. Also, as a result of π-π interactions, their tendency to form an excited state dimer (excimer) increases. These disadvantages can be overcome by doping into the host material or synthetic modifications. There are many studies in the literature using one or both methods.

Table 1.1 Perylene based OLED literature

Ref	Molecule	HOMO - LUMO Level (eV)	OLED Device architecture	EQE (%)	$V_{turn-on}$ (V)	CIE (x, y)
46	PDI1	-6.06, −4.08	ITO/PEDOT:PSS/PDI1/Al	-	-	-
	PDI2	-5.84, -4.11	ITO/PEDOT:PSS/PDI2/Al	-	-	-
	PDI3	-5.69, -4.13	ITO/PEDOT:PSS/PDI3/Al	-	-	-
47	STPH	-5.68, -3.77	ITO/P:P/CBP:**STPH**/TmPyPB /Liq/Al	3.97	8.3 *	(0.56, 0.37)
	DTPH	-5.75, -3.75	ITO/P:P/CBP:**DTPH** /TmPyPB /Liq /Al	4.30	7.6*	(0.57, 0.32)
	STRPH	-5.85, -3.76	ITO/ P:P /CBP:**STPH**/TmPyPB /Liq /Al	4.93	7.5*	(0.56, 0.34)
	DTRPH	-5.77, -3.77	ITO/P:P/CBP:**DTRPH**/TmPyPB/Liq/Al	3.52	8.2*	(0.57, 0.31)
	STTPE	-5.72, -3.75	ITO/ P:P/CBP:**STTPE**/TmPyPB/Liq/Al	0.50	4.5*	(0.50, 0.32)
	DTTPE	-5.80, -3.80	ITO/P:P/CBP:**DTTPE**/TmPyPB/Liq/Al	0.49	8.8*	(0.51, 0.24)
48	PEIs-1	-5.66, -3.38	ITO/P:P/PVK:1/2/3(15:1)/BPhen/LiF/Al	-	5.30	(0.48, 0.42)
	PEIs-2	-5.84, -3.42		-	6.08	(0.50, 0.43)
	PEIs-3	-5.86, -3.42		-	6.97	(0.47, 0.40)
	PEIs-1	-5.66, -3.38	ITO/ P:P /PVK:1/2/3(15:1)/TPBi/LiF/Al	-	3.68	(0.56, 0.42)
	PEIs-2	-5.84, -3.42		-	3.94	(0.36, 0.33)
	PEIs-3	-5.86, -3.42		-	4.29	(0.37, 0.31)
49	Molecule **1**	-5.59, -3.25	ITO/ P:P /**1**/BCP/Alq3/LiF /Al	1.76	6.16	(0.32, 0.56)
			ITO/ P:P /PVK: 1(10 wt.%)/BCP/Alq3 /LiF /Al	2.57	4.97	(0.33, 0.54)
50	Molecule 1	-5.72, -3.28	ITO/ P:P /Molecule(1–3) /BPhen /LiF/Al	-	3.52	-
	Molecule 2	-6.08, -3.07		-	3.96	-

Ref	Molecule	HOMO - LUMO Level (eV)	OLED Device architecture	EQE (%)	$V_{turn-on}$ (V)	CIE (x, y)
	Molecule 3	-6.04, -3.10		-	4.03	-
	Molecule 1	-5.72, -3.28	ITO/ P:P /PVK:Molecule(1–3)(90:10) /BPhen /LiF/Al	-	4.8	-
	Molecule 2	-6.08, -3.07		-	5.9	-
	Molecule 3	-6.04, -3.10		-	6.7	-
51	PDI-1	-5.8, -3.7	ITO/ P:P /PVKc/PDI-1/PF-PEG/Ba/Al	0.24	6.5	(0.66, 0.33)
	PDI-2	-5.5, -3.6	ITO/ P:P /PVKc/PDI-2/PF-PEG/Ba/Al	0.64	4	(0.69, 0.29)
52	PDI-1BN	−4.8, −3.63	ITO/MoO$_3$ /TCTA /CBP: X wt % PDI-1BN /TPBi /LiF/Al	1.57	3.5	-
53	N-DODEPER	-5.9, -3.7	ITO/ P:P /PVK:N-DODEPER(% 0.2, 0.4 and 0.8 N-DODEPPER)/Alq3/LiF /Al	0.78	4,5	(0.28, 0.54)
54	PDI-1	-6.0, -3,8	ITO/ P:P /PVK-PBD-PDI-1/Ba/Ag	0.09	12*	-
	PDI-2	-5.4, -3.5	ITO/ P:P /PVK-TPBI-PDI-2/Ba/Ag	0.62	12*	0.65, 0.35
55	[PDI-iridium]PF6 dyad 1	-5.5, -3.18	ITO/ P:P /1:IL(2:1)/Al	3.27	3*	(0.65, 0.34)
56	BNPTCD	-6.1, -4.0	ITO/m-MTDATA/-NPD/Alq3:BNPTCD(61:39)mol%/LiF/Al	0.002	6.4	-

Operation Voltage, - Not reported. P:P= PEDOT:PSS, BCP =2,9-Dimethyl-4,7-diphenyl-1,10-phenanthroline, Alq3= Aluminum 8-hydroxyquinolinate, PVK= Poly(9-vinylcarbazole), BPhen= 4,7-Diphenyl-1,10-phenanthroline, TCTA= Tris(4-carbazoyl-9-ylphenyl)amine, CBP= 4,4'-Bis(9-carbazolyl)-1,1'-biphenyl, TPBi= 2,2',2"-(1,3,5-Benzinetriyl)-tris(1-phenyl-1-H-benzimidazole), m-MTDATA= 4,4',4"-Tris[(3-methylphenyl)phenylamino]triphenylamine, LiF= Lithium fluoride,

To give an example from the literature, in a study, 3 new acetylene bridges perylenediimide derivative were functionalized with fluorene, carbazolyl-fluorene, and anthracyl-fluorene derivatives and their optical and electrochemical properties were investigated. Among the added groups, the fluorene-containing PDI derivative prevented aggregation. Device performance data are not reported. In addition, they reported an EL device containing PDI in a plasmonic-enhanced device with the addition of nanowires [46]. In another study, different PDI derivatives with stiff bulky structures were synthesized by functionalization from the bay position and red shifted PL observed. After their optical electrical characterization, OLED was produced with the use of PDIs in the active layer. OLED devices fabricated by adding 1% and 5% PDI to the CBP host, the highest EQE (4.93%) was obtained by adding 1% STRPH coded PDI derivative to obtain a deep red

EL [47]. In another study, PVK and bay annulated PTE derivatives were used together in a host-guest system, the effects of the device with the use of (ethyl) amine, sulphur and selenium derivative fused in the PTE core in the active layer were investigated. While the (ethyl) amine fused-PTE derivative exhibited maximum brightness of 265.82 cd/m^2 by the use of BPhen as an electron transfer material, sulphur and selenium derived exhibited 82.8 and 19.31 cd/m^2, respectively. Subsequently, using TPBi instead of Bphen as ETL in Device architecture, the Turn-On voltage for (ethyl) amine fused-PTE decreased from 5.30 to 3.68 and brightness increased from 265.82 to 628. In addition, blue EL from PVK was mostly realized by the (ethyl) amine derivatized material using due to förster resonance energy transfer (FRET). The CIE coordination (x, y) of the produced device performances (where ETL: TPBi) are (at 14V) ((ethyl) amine, sulfur and selenium derived-PTE) (0.50, 0.42), (0 .39, 0.38), (0.32, 0.28), respectively[48]. In another study they used a new TADF-derived perylene derivative material, functionalized with the triazine molecule, which is electron-weak in the center, and the N-ring PTE derivative from the electron-rich bay position utilized in 2 different device structures. In the first, OLED fabricated with ITO (120 nm) / PEDOT: PSS (50 nm) / Perylene derivative (80 nm) / BCP (6 nm) / Alq3 (35 nm) / LiF (1 nm) / Al (150 nm) structure and Vturn-on (V) 6.16, maximum brightness 4334cd /m2, 2.04 lmW^{-1} power efficiency and 1.76% EQE were obtained. ITO (120 nm) / PEDOT: PSS (50 nm) / PVK: 1 (80 nm) / BCP (6 nm) / Alq3 (35 nm) / LiF (1 nm) / Al (120 nm) device architecture was fabricated and Von 4.97, 5561cd / m2 brightness, 3.34 lm / W and 2.57% EQE were achieved[49]. In a study comparing the OLED device performances of PTE derivatives functionalized with heteroatom (NH, S, Se) showed liquid crystal properties, all PTE derivatives exhibited a 200-300 degree columnar phase at room temperature. OLED device fabricated PTEs alone in the active layer performed lower than when they were added to PVK. N-ring PTE derivative added 10% into the PVK host exhibited 211cd/m2 brightness in green region and 0.27cd/A current efficiency [50]. In the study conducted by Enrika et al. in 2016, two different perylene diimide derivatives were synthesized and solution phase OLED was fabricated. Naphthalene or acenaphthene bond to the bay position of perylene diimide prevents aggregation by limiting π-π interactions. In this study with ITO/ PEDOT:PPS/PVKc/PDI/PF-PEG/Ba/Al device architecture, 0.638 and 0.238 EQE were obtained [51]. BN-Fused Perylene diimide was synthesized and characterized in the study by Li et al. Made with ITO/MoO3/TCTA/CBP: X wt % PDI-1BN/TPBi/LiF/Al device

architecture reached 1.57 EQE value. Many other studies based on perylene diimide are available and are summarized in table 1.1.

In most of the studies summarized in Table 1.1, perylene diimide was added to a host. Strong π-π interactions of perylene diimides cause film phase aggregation. Therefore, it is difficult to get high efficiency by coating them individually. They are doped into a host for efficient energy end charge transfer. As host materials generally have high band gap, they are generally used for blue emission, energy and charge transfer. These materials generally exhibit p-type or n-type character with exceptions. Due to these uniform characters, it may be difficult to balance the charge in the active layer. This problem can be overcome by using p-type and n-type materials together. PVK, is a p-type host and widely used due to its excellent film-forming properties in studies with wet coating methods. Kumar et al. mixed PVK with n-type material of OXD-7 and achieved high efficiency in their study [57]. Similarly, PVK: PBD [58–60], PVK:mCP [61,62], PO:TCTA [63], TCTA:DBFTrz, CBP:TPBI, CBP:DBFTrz [64] blends are also utilized literature.

1.6. Aim of The Thesis

The aim of this thesis is to obtain high quality white light with a CRI value higher than 90 by utilizing perylene derivatives as singlet emitters in a solution processed single layer WOLED. For this purpose, different host materials were blended with the previously synthesized orange-red and green emitting perylene derivatives and photophysics and physics of the devices were investigated.

CHAPTER 2

EXPERIMENTAL

2.1. Materials

Orange-red emitting material of N,N'-bis(2-ethylhexyl)perylene-3,4,9,10-dicarboxylic diimide (PDI) and green emitting material of perylene-3,4,9,10-tetracarboxy tetrabutylester (PTE) were sensitized and characterized by Dr. Erkan AKSOY in his PhD thesis[65,66]. Indium tin oxide (ITO) coated glass substrates with a sheet resistance of 4-10 Ω/sq are utilized as transparent anode and were purchased from Lumtec. Hydrochloric acid (%30-32) [$HCl_{(aq)}$] was purchased from Tekkim, poly(3,4-ethylenedioxythiophene):poly(styrene sulfonate) (PEDOT:PSS, Al4083) was from Heraeus Clevios, poly (N-vinylcarbazole) (PVK) (Mw 1.100.000), 2-(4-Biphenylyl)-5-phenyl-1,3,4-oxadiazole (PBD), 1,3-bis[(4-tert-butylphenyl)-1,3,4-oxadiazolyl]phenylene (OXD-7), aluminium (Al), chlorobenzene, isopropanol and acetone were from Sigma Aldrich. Lithium fluoride (LiF) was provided from Acros Organics.

2.2. Instruments

Ultraviolet-visible (UV-Vis) absorption and photoluminescence (PL) measurements were performed by using Edinburgh Instruments FS5 spectrophotometer. ITO substrate cleaning was processed by ISOLAB ultrasonic bath and CUTE FC-10046 O_2 plasma system. All solutions were coated via Laurell WS-400B-6NPP LITE spin coater under atmospheric conditions. Film thickness values were determined by KlaTencor MicroXM-100 optical profilometer. Surface morphology investigations were carried out with Bruker-MMSPM Nanoscope 8 atomic force microscopy (AFM). Cathode and electron injection layer (EIL) evaporations were performed by the use of a physical vapor deposition (PVD) instrument attached to a LC Technology Solution Inc. glove box system. Coating thickness and rate were monitored by INFICON SCQ-310C deposition controller by using a 6 MHz crystal sensor and frequency meter together with quartz oscillator which allowed controlling rate by 0.1 Å/s. EL spectra and luminance–voltage–

current density (L–V–J) curves were obtained using a Keithley 2400 programmable source measurement unit and calibrated Hamamatsu C9920-12 measurement system combined with an integrated sphere (inside diameter of 3.3 inch). The detector and the sphere were connected with 1.5 m fiber cable.

2.3. Device Preparation

Before coating organic materials, ITO coated glasses were appropriately etched with $HCl_{(aq)}$ and cleaned with detergent, water, deionize water, acetone and isopropyl alcohol, respectively for half an hour each, by using ultrasonic bath. After ultrasonication, ITO coated glass substrates were dried with a nitrogen gun then O_2 plasma (70W) treatment applied for 8 minutes to remove residual contamination and make surface hydrophilic. PEDOT:PSS was filtered through a RC 0.45µm filter then coated by using spin coater (3000 rpm, 1 minute) and annealed at 100°C for 30 minutes. Active layer (Emitting Material Layer: EML) was also spin coated on top of PEDOT:PSS at 3000 rpm for 1 minute and annealed at 125°C for 30 minutes. Finally, LiF (1 nm) and Al (100 nm) cathodes were deposited through a shadow mask and by the use of vacuum evaporator at 10^{-6} torr and deposition rates of LiF and Al were 0.2 Å /s and 2.5 Å/s, respectively.
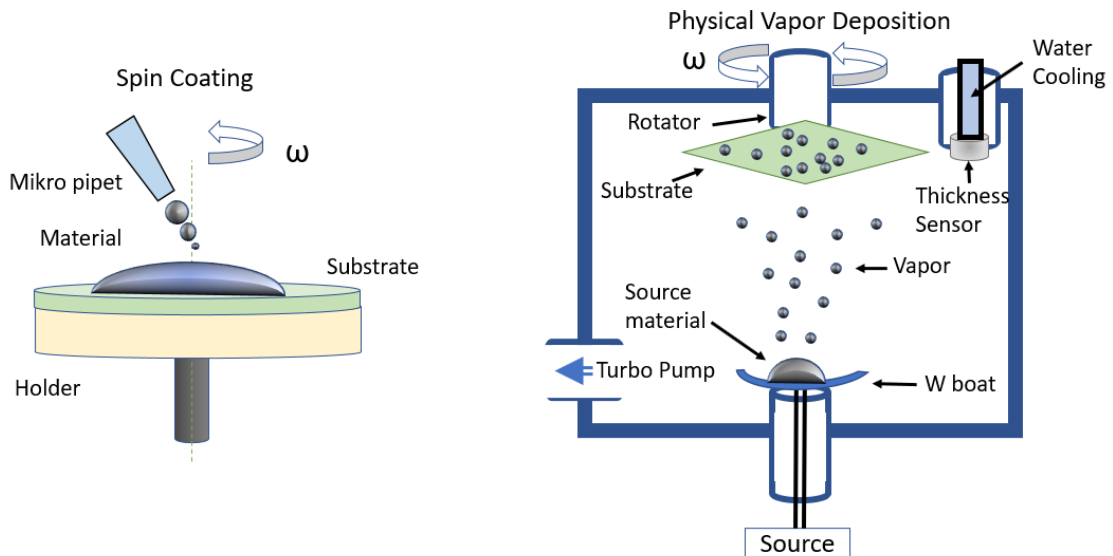

Figure 2.1 Coating techniques used in this work

All of OLED devices presented in this thesis has basic device structure of ITO/PEDOT:PSS/EML/LiF/Al with active areas of 7 mm^2. Light emitting layer solutions of x wt.% PDI, x wt.% PTE or x wt.% PDI:PTE (for PDI x= 0.03, 0.06, 0.1, 0.2, 0.4,

0.6, 0.8, 1.0 for PTE x= 0.03, 0.06, 0.1, 0.20 and for PDI:PTE x= 0.1:0.03, 0.1:0.06, 0.1:0.1, 0.06:0.03) in host matrices of PVK:PBD or PVK:OXD-7 (60:40 wt.%) were prepared in chlorobenzene and stirred overnight. Total solution density was kept as 30 mg/mL for each of them. Six parallel devices were fabricated for each EML and mean efficiency values are presented in the thesis.

CHAPTER 3

RESULTS AND DISCUSSIONS

Device characteristics of orange-red (OR) emitting OLEDs prepared in two different host matrices and with varied PDI content are presented, in sections 3.1 and 3.2, respectively. Section 3.3 presents the device characteristics and related discussions of bare PTE and PTE introduced OR-OLEDs where PDI wt% was kept constant. Finally, in section 3.4 optimization of WOLED characteristics through PTE and PDI wt% in the emissive layer is presented together with the stability experiments.

3.1. Characterization and Determination of Host

In organic light emitting diodes, electrons and holes are transmitted from opposite electrodes must be reach at emitter material at the same time with balanced ratio in order to work efficiently. If a single material is used, that must be ambipolar. Only in this case, capacity to carry electrons and holes must be equal, which is rare. Another way of transmitting electrons and holes to the emission material is to blend two host at an appropriate rate. Among the host materials that can carry holes, PVK is the first material that comes to mind with its good film forming properties and compatible energy levels [67], [61]. However, because of low-lying HOMO level of PDI and having low electron mobility of PVK , bare PVK cannot be considered as an ideal host [54]. Therefore, in order to enhance electronic level alignment and also increase the electron density in the emissive layer, two dopants with different electron mobility values were also introduced in the PVK layer. Oxadiazoles has been used frequently as electron transfer material since the early 1990s and has been well-studied so far such as PBD [68] and OXD-7 [69] . OXD-7 and PBD with electron mobility values of $1–4 \times 10^{-5}$ and 8×10^{-7} cm^2 V^{-1} s^{-1}, respectively [70]. Energy levels of the materials are depicted in figure 3.1 together with the open structures of PDI and PTE. Film morphology plays an important role for OLED, especially in terms of charge transfer process, thus knowing the surface morphology is crucial. Surface roughness is monitored by the RMS value considering the peaks and valleys on the thin film. The AFM micrographs of PVK:PBD (RMS of 0.31) and

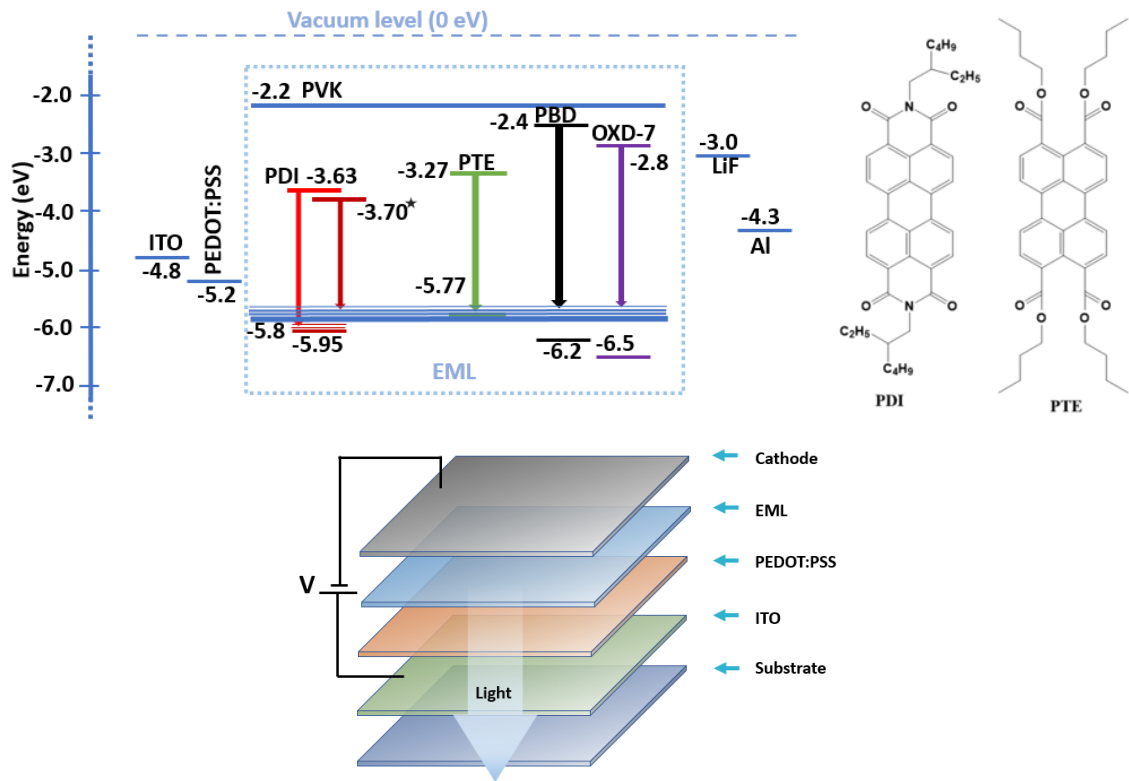PVK:OXD-7 (RMS of 0.44) films presented homogenous and quite smooth surfaces(figure 3.2).

Figure 3.1. Energy band diagram of the devices, chemical structure of PTE and PDI and device architecture [energy levels of PVK [50], OXD-7 [71], PBD [72], are taken from literature and PTE and PDI are calculated by using the first reduction potentials by the use of cyclic voltammetry and optical band gaps [66].
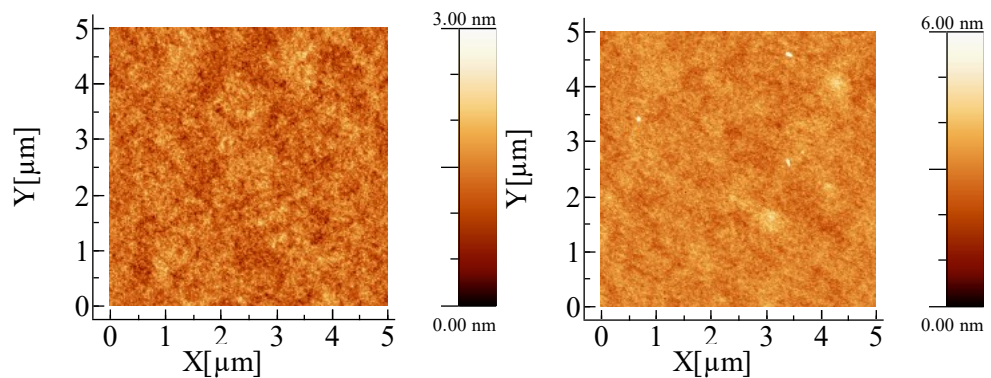

Figure 3.2. AFM images of PVK:PBD(left) and PVK:OXD-7(right) films.

For bare PDI containing devices, PVK:OXD-7 host presented lower current density and luminance values, and higher turn-on voltages ($V_{turn-on}$) (figure 3.3 a and b)

than those of PVK:PBD host. Lower current density and luminance values are attributed to the lower HOMO and LUMO energy levels of OXD-7 (figure 3.1). Lower HOMO level may act as a trap center for the injected holes, whereas the latter may have caused an unnecessarily high electron injection in to the emissive layer. In order to confirm this suggestion current density-voltage characteristics of hole and electron only devices are compared.
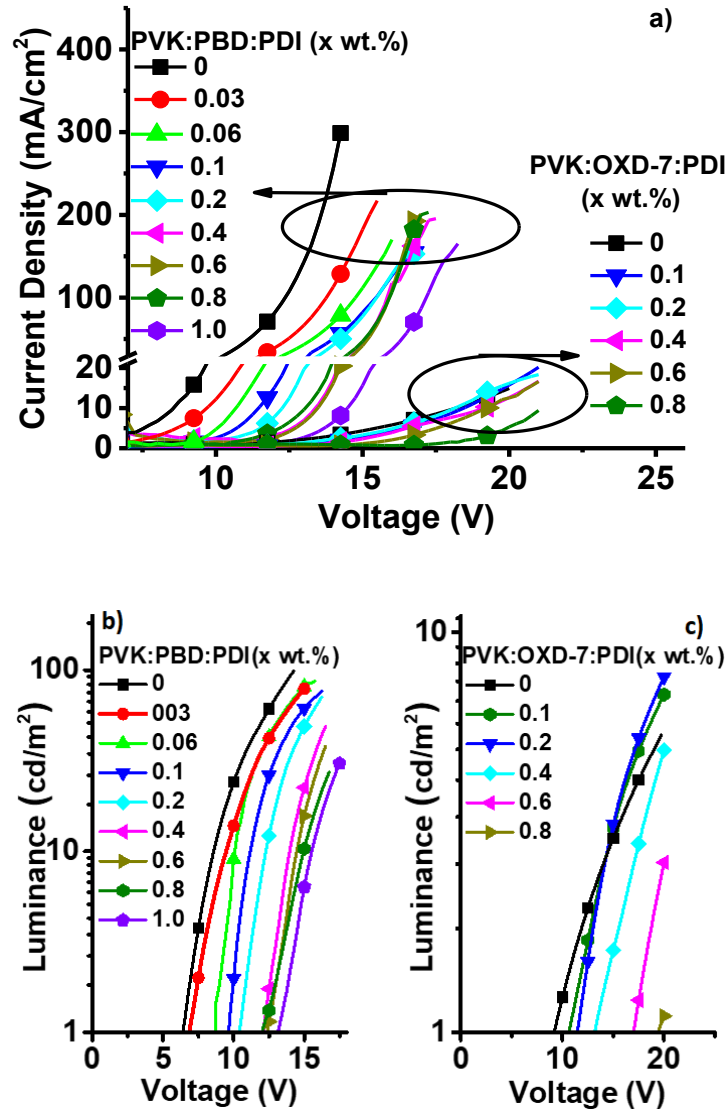

Figure 3.3. a) Current density (J)- Voltage (V) and b) Luminance (L)-Voltage (V) characteristic of bare PDI devices in host matrices of PVK:PBD and PVK:OXD-7.

Mobility is defined as the speed of charge carriers under applied electric field. According to carrier mechanism, recombination zone will be closer to low mobility side. Therefore, detecting the electron and hole mobility gives information about the recombination zone and also facilitates the adjustment of it. ITO/PEDOT:PSS/Active

22

Layer/Au and Al/Active Layer/LiF/Al devices are prepared to detect hole and for electron mobility values, respectively. Working principle is summarized in figure 3.4 and the current density-voltage curves are presented at appendix A.
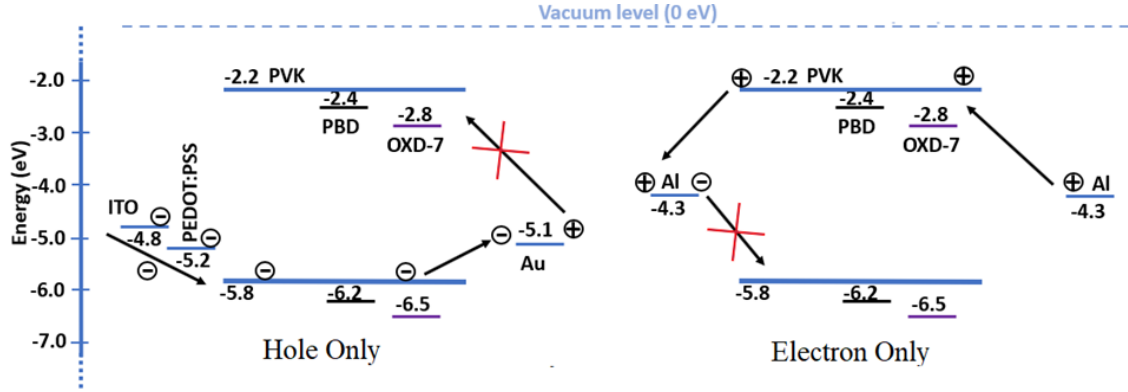

Figure 3.4 Hole only (left) and electron only (right) device working principle

Electron and hole mobility were calculated using drift regime (Mott-Gurney law) as discussed before. Frequency-varying capacitance values were determined up to 10^6 Hz. Permittivity and mobility were found according to following equation [73].

$$C = \frac{\varepsilon A}{d}, \qquad \mu = \frac{J_{SCLC}}{V^2} d^3 \frac{8}{9\varepsilon} \qquad (3.1)$$

Since the film thickness (d) and area (A) are known and capacitance (C) is measured, the electrical permittivity (ε) of solid can be calculated. Hole mobility values of of PVK:PBD and PVK:OXD-7 are calculated to be 2×10^{-6} and 8×10^{-7} cm^{2}V^{-1}s^{-1}, respectively. Whereas, electron mobility of PVK:PBD is 8.7×10^{-7} and PVK:OXD-7 is 1.1×10^{-5} cm^{2}V^{-1}s^{-1}. These values confirms the above made suggestion on the effect of lower LUMO energy level of OXD-7. High electron mobility of OXD-7 and low hole mobility of PVK results charge imbalance in active area caused low luminescence.

In literature high working and driving potentials have been explained by the thicker emitting layers and the high void barrier at the PEDOT: PSS / PVK:OXD-7 interface [74]. Active layer thickness should be taken into account in OLEDs, the thickness of the layers is of great importance, which influence optical and electrical characterizations such as brightness and charge carrier transport [74–76] and consequently efficiency.
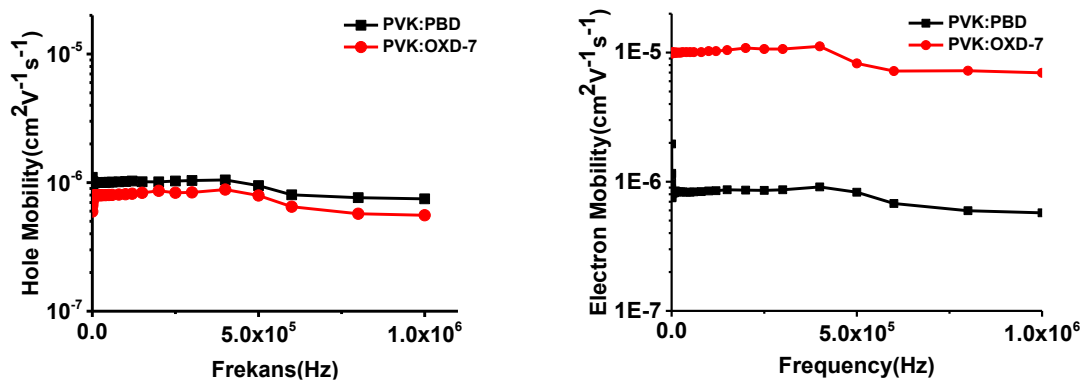
Figure 3.5 Hole only and electron only mechanism and charge carrier mobilities of PVK:PBD and PVK:OXD-7 hosts.

It has been shown that depending on the coating conditions and material properties efficiency values may increase with the increasing emissive layer thickness first and then dramatic decays can be monitored in case of further increment of the thickness [75]. Although the coating conditions and total concentration were the same, a dramatic difference in thickness was observed between the hosts (Appendix B). While PVK: PBD host matrix has an active layer thickness of 84±2.0 nm, PVK:OXD-7 active layer thickness determined to have an of 126±4.3nm. Higher thickness of PVK:OXD-7 layer may have caused charge accumulation on both sides of the active layer and resulted in an increased $V_{turn-on}$ for the PVK:OXD-7 based OLED [76].

Additionally, although the $V_{turn-on}$ values are increased with the increase in PDI doping wt% for both of the host media, this increment is more notable with PVK:OXD-7 host (figure 3.3). Above given explanation is also pertinent for the devices those of which PDI doping wt.% is increased. Presence of 0.1 wt.% PDI in PVK:OXD-7 caused approximately 10 nm of thickness increment whereas for PVK:PBD:PDI (0.1 wt.%) this increment is only 5 nm compared to their un-doped films. The thicknesses of PVK:OXD-7: PDI (0.1 wt.%) and PVK:PBD:PDI (0.1 wt.%) films are 135±4.9 nm and 89±3.4 nm, respectively (Appendix B). The huge thickness differences of the host media are attributed to the different molecular volumes and orientation of OXD-7 (378 Å^3) and PBD (270 Å^3) (molecules were drawn in the chemsketch software and their volumes were calculated by using an online tool [77]). Since electrons are located in certain regions of the molecules, the arrangement of the molecules can affect their electronic and optical properties. In cases of random orientation, electron density is randomly distributed and usability decreases, in case of organized orientation, the electron density will be high in

a local area and electronic properties improve. The horizontal orientation of the molecules both facilitates charge transfer and has a positive effect on light out coupling. OXD-7 has higher volume and less linearity compared to PBD. It can be said that this situation affects the coating thickness and electronic properties [78]. The $V_{turn-on}$ value increments obtained can also be explained by the high dipole moments and dipole moment differences of the hosts and PDI molecule which may create energy disorder and consequently reduce the carrier mobility and conductivity of the emitting layer [79]. Due to the comparatively better luminance and lower $V_{turn-on}$ values obtained, PVK:PBD was chosen as the host matrix.

3.2. Device Characteristic of Orange-Red Emitting OLEDs

The white light properties of the device structure of ITO/ PEDOT:PSS/ PVK:PBD:PDI (x wt%)/ LiF/ Al are summarized in table 3.1. The CIE coordinates of (0.36, 0.29), CTT of 4170 K and CRI of 90 could be reached with 0.1wt%PDI doping.

Table 3.1. PDI doping wt% dependent CRI, CCT and CIE values of ITO/ PEDOT:PSS/ PVK:PBD:PDI (x wt%)/ LiF/ Al devices.

	PVK:PBD:PDI (wt%)						
	0.06	0.1	0.2	0.4	0.6	0.8	1.0
CRI	86	90	82	80	76	74	69
CCT	7901	4170	3711	2558	2431	2276	2333
CIE	0.32, 0.26	0.36, 0.29	0.41, 0.34	0.43, 0.35	0.44, 0.35	0.45, 0.35	0.45, 0.35

The EL maximum of PVK:PBD host presented 15 nm of red shift compared to its PL as a result of exciplex emission [60]. The orange-red region of the EL was mainly dominated by a peak at 610nm (figure 3.6a). Generally, this peak has been observed in PL spectrum of bare PDI films and attributed to aggregation of the PDI core due to π-π stacking [47]. However, 0.1 wt% of PDI content corresponds approximately 5×10^{-5} M of PDI concentration and aggregation induced PL behavior might not be expected. Therefore, PL measurements are carried on in order to further understand the mechanism and origin of this peak. PL spectra of PVK:PBD:(0.1 wt%)PDI film presented the same emission wavelength maxima (λ^1_{ems}=551 nm, λ^2_{ems}=598 nm and λ^3_{ems}=650 nm) of PDI (figure 3.6a) with the excitation wavelengths of 510 nm and 310 nm which were used for

the excitation of the PDI and host, respectively. Although they preserved characteristic three peak decreasing intensity structure of PDI, λ_{ems} maxima and PL offset were red shifted approximately 20 nm and 90 nm, respectively, compared to the solution phase ($[10^{-6}]$ in chloroform) and polystyrene (PS): 0.1 wt% PDI film (figure 3.6b). These shifts are evaluated as possible formation of another excited state.
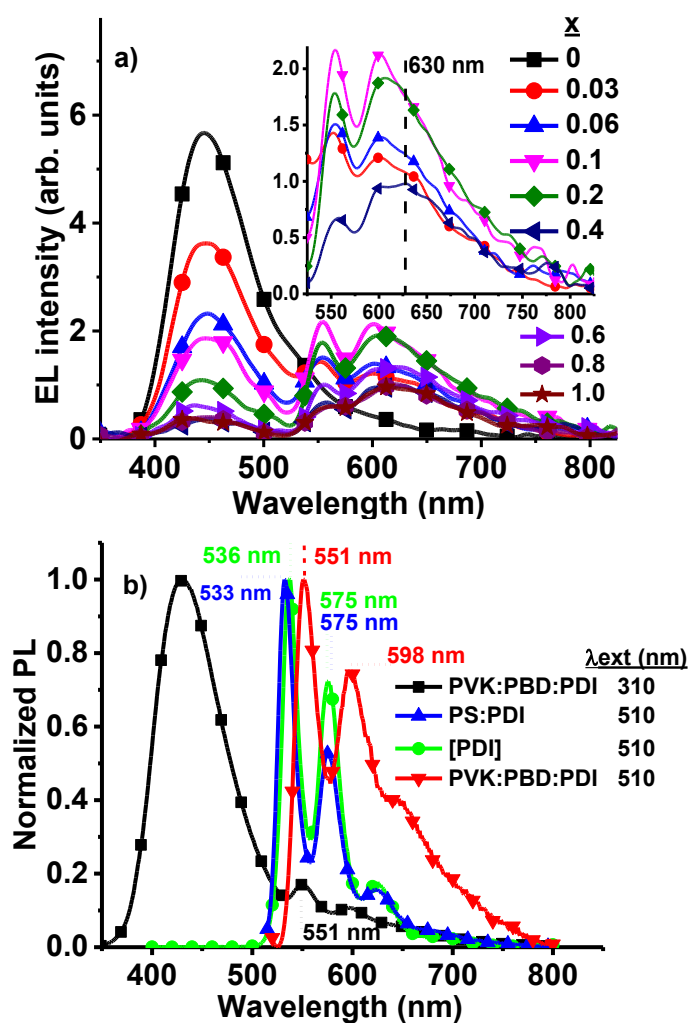

Figure 3.6. a) EL vs wavelength spectra of PVK:PBD:x wt%PDI devices (*inset*: EL intensity change at orange-red region for the x values between 0.03 and 0.4) and b) PL curves of polystyren (PS):PDI , PS:PVK:PBD:PDI, films and PDI solution in CHCl$_3$.

Interestingly, in the EL spectrum, λ^1_{ems} of PDI was the same while λ^2_{ems} of it has also presented approximately 15 nm of red shift and gave a peak at 610 nm. It is deduced that the EL obtained at 610 nm was a result of an excited/ground state energy or charge transfer interaction between the host and PDI. In applied voltage dependent EL measurements [80–82] arising of a new peak at 630 nm is observed and intensities of both

the blue and the orange-red regions are affected equally from the voltage increments (figure 3.7b). Therefore, it is suggested that the EL at 610 nm was actually the combination of λ^2_{ems} of PDI and exciplex (electron-hole hetoropairs) emission with a peak point at 630 nm. This suggestion is supported by the EL intensity increments observed at 630 nm with the increase in PDI doping wt% in PVK:PBD host system (figure 3.7a, inset).
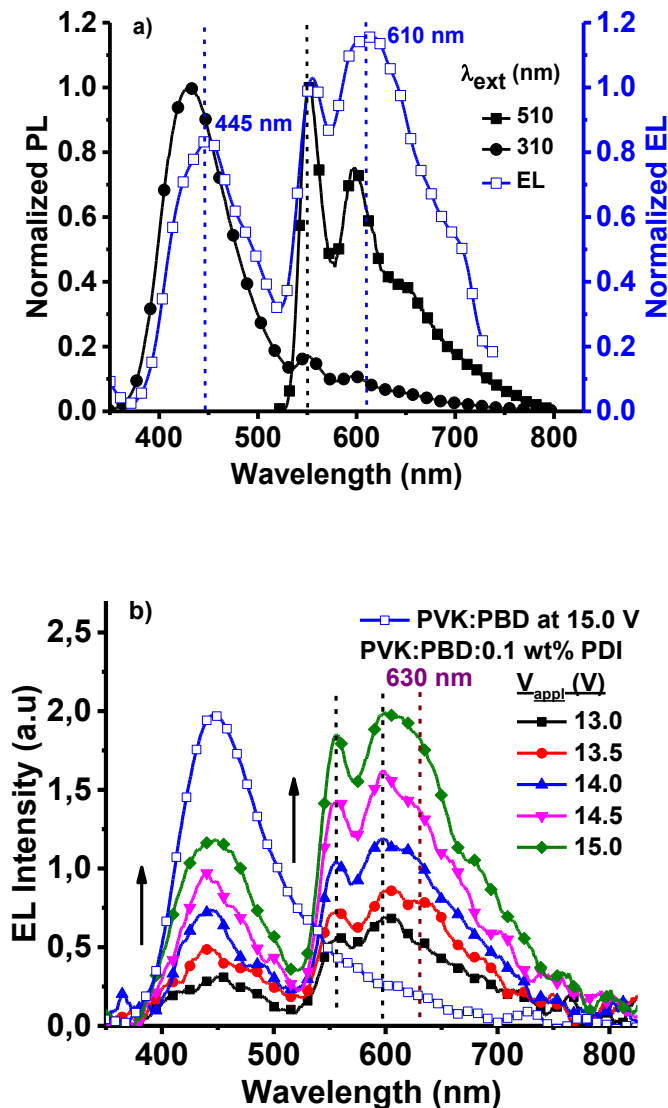

Figure 3.7. a) Normalized PL and EL spectra of PVK:PBD:PDI (0.1 wt%) (Vappl=15 V) and its corresponding WOLED, respectively and b) applied voltage dependent EL spectra of the device with PVK:PBD:PDI (0.1 wt%) emitting layer together with the EL spectrum of bare PVK:PBD device.

3.3. Device Characteristic of Green Emitting OLEDs

In order to increase the visible light region coverage and consequently, CRI value of bare orange-red emitting PDI containing devices, green light emitting PTE is thought to be introduced in the emission layer. A forehand, the behavior of ITO/ PEDOT:PSS/ PVK:PBD:PTE(x wt%)/ LiF/ Al device is monitored. In a similar manner with the bare PDI devices, the $V_{turn-on}$ values increased with the increasing doping ratio of PTE (figure 3.8) but the maximum luminance value produced by the bare PTE containing device was slightly higher than that of the bare PDI containing one (figure 3.8 vs 3.3 b and c). This is attributed to more efficient energy transfer from the host to PTE due to bigger integral area (overlap) between the absorption of it and emission of PVK:PBD compared to that of PDI. Absorption and emission spectra of PVK:PBD, PDI and PTE are provided in Figure 3.9b.. It is well known that in host:guest systems the emission is usually controlled by energy transfer (Förster or Dexter mechanism) between them [83].
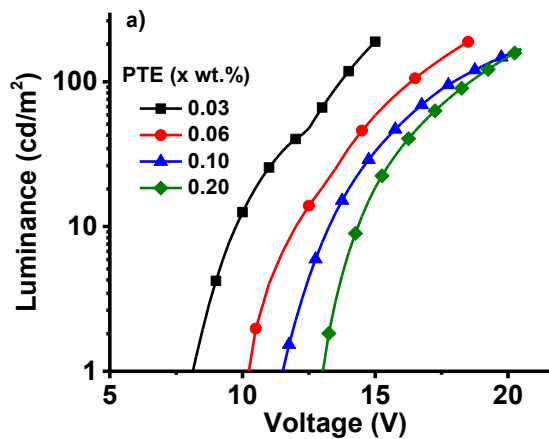

Figure 3.8. L-V characteristic of active layer of PVK:PBD:PTE

The measure of energy transfer is supported by steady state quenching experiments. PDI and PTE were used as quenchers for the emission of PVK:PBD host and quenching rate constants of $9x10^{10}$ s^{-1} and $3.6x10^{11}$ s^{-1}, respectively were extracted from the corresponding Stern-Volmer plots (Figure 3.9a). This method provides information on degree of the intermolecular kinetic interaction. It explains the effect of another species in the molecule and situation in which the kinetic photophysical interaction will be deactivate. It was determined by following equation;

$$\frac{I_0}{I} = 1 + k_q \tau_0 Q \qquad (3.2)$$

where I_0 is initial PL intensity, I is after adding quencher, k_q is rate constant, τ_0 is life time of host and Q is concentration of quencher. The rate constants were calculated to be higher than the diffusion control limit of 10^{10} and suggested a possible charge transfer process between the carbazole based host and perylene derivatives [51].
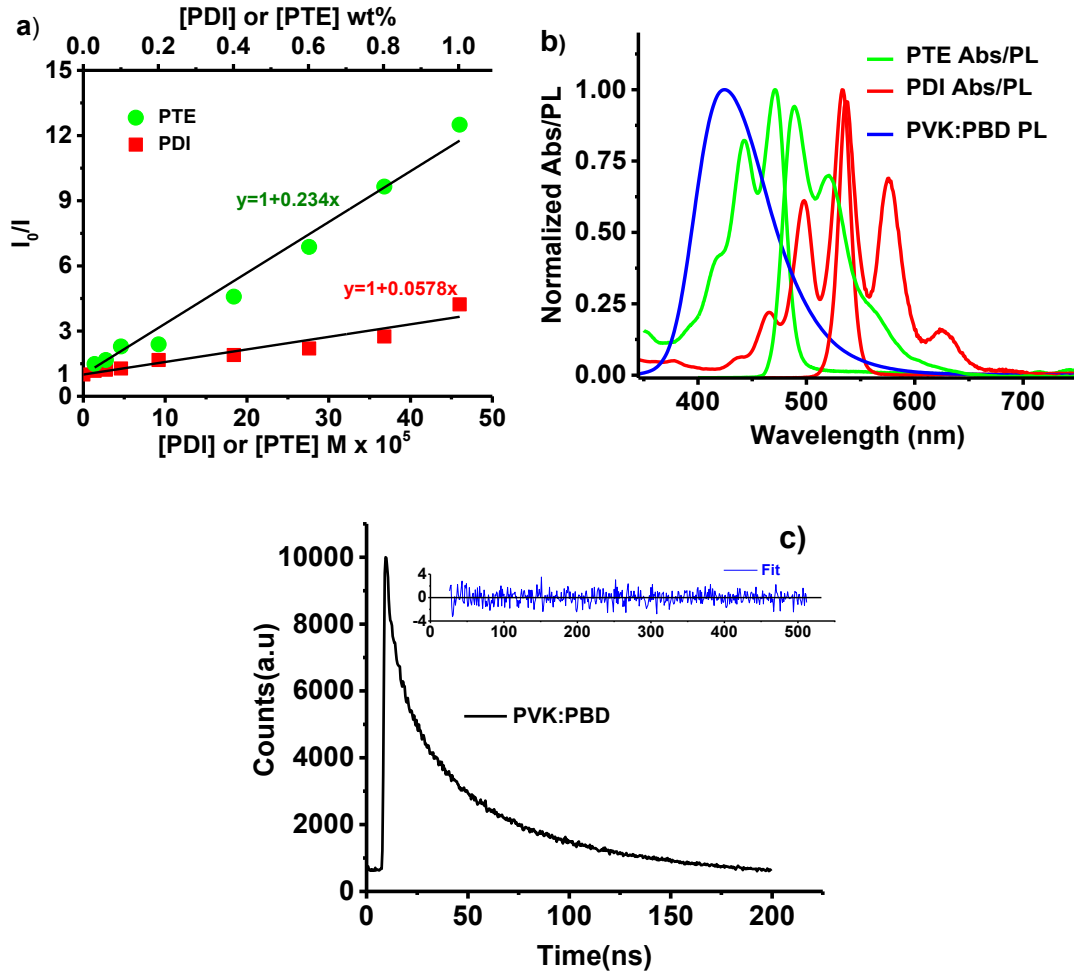

Figure 3.9 a) Stern Volmer plot of PVK:PBD quenching with the addition of PDI and PTE by wt.% and M in film phase b) Absorption emission spectrum of PDI and PTE and emission spectrum of PVK:PBD c) average radiative life of PVK:PBD (measured as 65 ns).

As a result of better energy transfer from the host to PTE, the ratio needed to obtain white light was much lower than that of the PDI. The devices that contain 0.03, 0.06 and 0.1 wt% PTE presented greenish white light and the CIE values remained above the Planckian locus (black body locus) while for the bare PDI devices these values were below it (Figure 3.10). Further increment of PTE wt% did not cause a significant change in the EL intensities of blue and green regions (figure 3.11a).

Table 3.2. PTE doping wt% dependent CRI, CCT and CIE values of ITO/ PEDOT:PSS/ PVK:PBD:PTE (x wt%)/ LiF/ Al devices

	PVK:PBD:PTE (wt%)			
	0.03	**0.06**	**0.1**	**0.2**
CRI	77	74	71	65
CCT	7094	5402	5154	4860
CIE	0.29, 0.37	0.34, 0.42	0.35, 0.45	0.37, 0.49

The green region of the EL was dominated by a peak at 535 nm which corresponds to a wavelength of 15nm red shifted second PL peak of PTE in solution phase (λ^2_{ems}=520 nm figure 3.8c). The intensity of 535 nm peak is increased with PTE doping wt%. Both the red shifted peak and increasing EL intensity behaviors were similar to the situation in PDI. However, unlike the case in PVK:PBD:PDI devices, the applied voltage dependent EL spectra presented significant intensity differences between the blue and green regions; the intensity of 535 nm peak increased more than two folds of the 445 nm peak (Figure 3.11 c and d). There are differences between PL and EL spectrum of PTE. Considering PTE concentration, there are two possible causes for this exciplex or electroplex. When the voltage-dependent EL spectrum is examined, it is seen that there is a voltage-dependent behaviour. This is proof of electroplex formation. Therefore, it is suggested that the EL peak of 535 nm was a result of electroplex formation between the host and PTE [80–82].
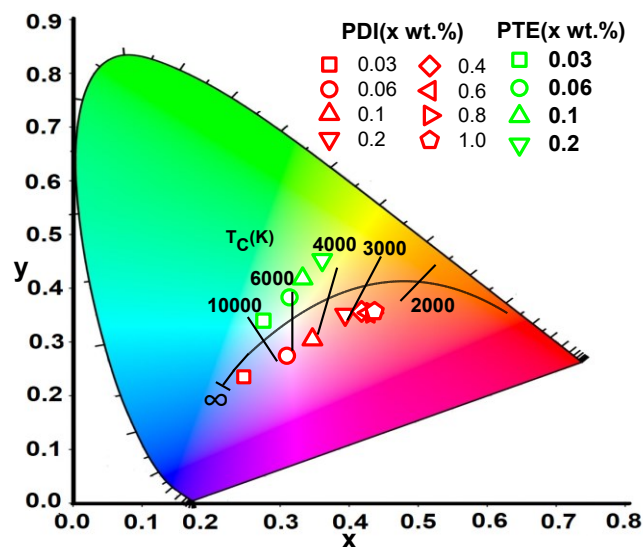

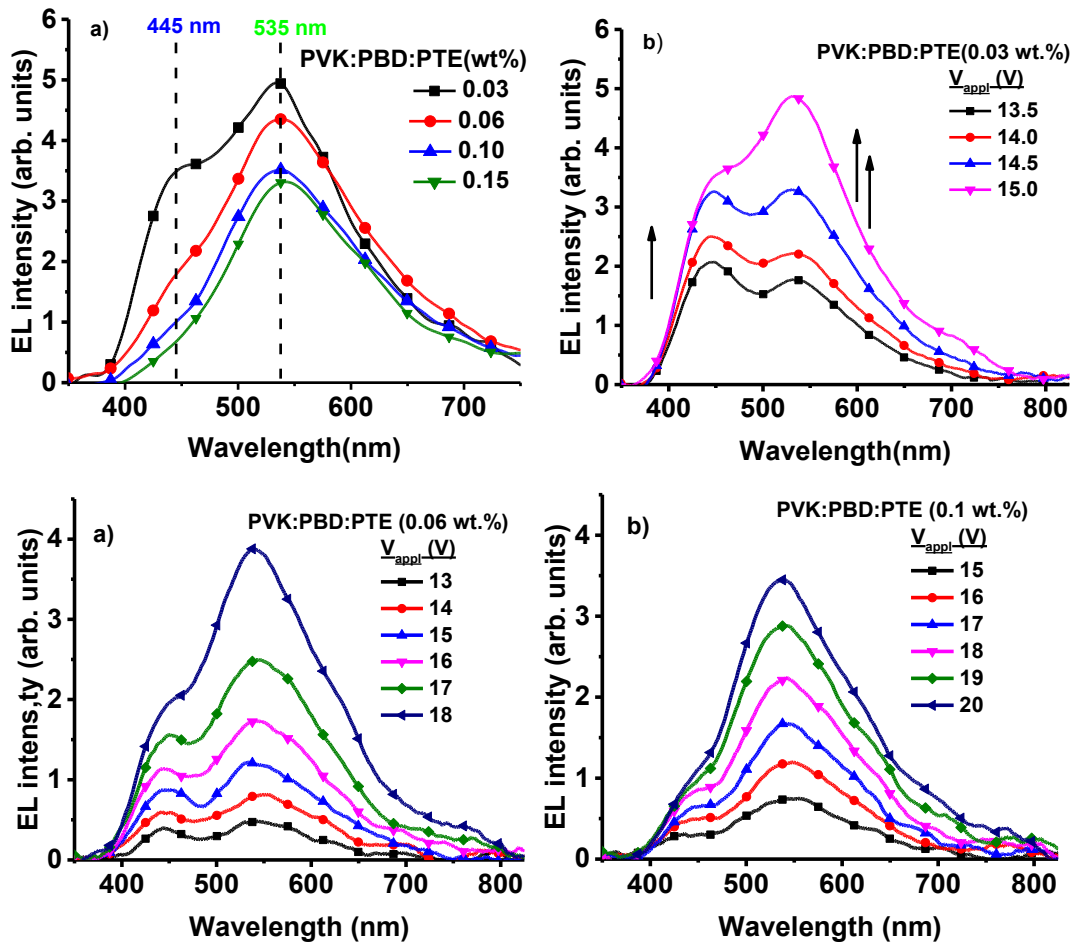Figure 3.10. Chromaticity diagram of the devices containing PVK:PBD:PDI and PVK:PBD:PTE emission layers.

Figure 3.11. a) EL spectra of PVK:PBD:x wt%PTE devices and applied voltage dependent EL spectra of the device with PVK:PBD:PTE (x wt%) b) x=0.03, c) x=0.06, d) x=0.1 emitting layer.

Although the CRI values were only around 75 because of the lack of orange-red region, within the PTE containing devices CIE and CCT values of PTE wt %<0.1 devices presented the closest values to white light (Table 3.2).

3.4. Device Characteristic of WOLEDs

Until this section, host, PDI and PTE ratios have been optimized. Here, PDI and PTE were used together to enhance the quality of white light. In the study with PTE, it was seen that the CRI value was less than the study with PDI. The CRI value reached the highest value when 0.1 wt.% PDI. Therefore, doping ratios of PTE were considered to be introduced in the 0.1wt.%PDI containing device. Device configuration of ITO/PEDOT:PSS/PVK:PBD:PDI (0.1wt%): PTE (x wt)/LiF/Al (x= 0.03 Device 1, x=0.06 Device 2 and x=0.1 Device 3) was employed. As expected, an increment and a

decrement at the green and blue regions, respectively of the EL spectra are detected as the wt % of PTE is increased (figure 3.12a). Fading of 630 nm emission of bare PDI device and disappearance of the electroplex peak at 535 nm in bare PTE devices are also monitored. The $V_{turn-on}$ values of Device 1-3 were in the range of bare PDI and bare PTE containing devices. Although the current density at the same applied voltage is in the order of Device 1>Device 2 = Device 3 (figure 3.12b), the EL intensity decrement at 630 nm is continued in Device 2 and Device 3. This situation is evaluated as another evidence of electric field independent formation of 630 nm peak and the fading is ascribed to the reduction of host concentration ready to form exciplex with PDI as the PTE wt% is increased. Absence of 535 nm peak is attributed to the wide overlap between the emission of PTE and absorption of PDI (figure 3.9c).
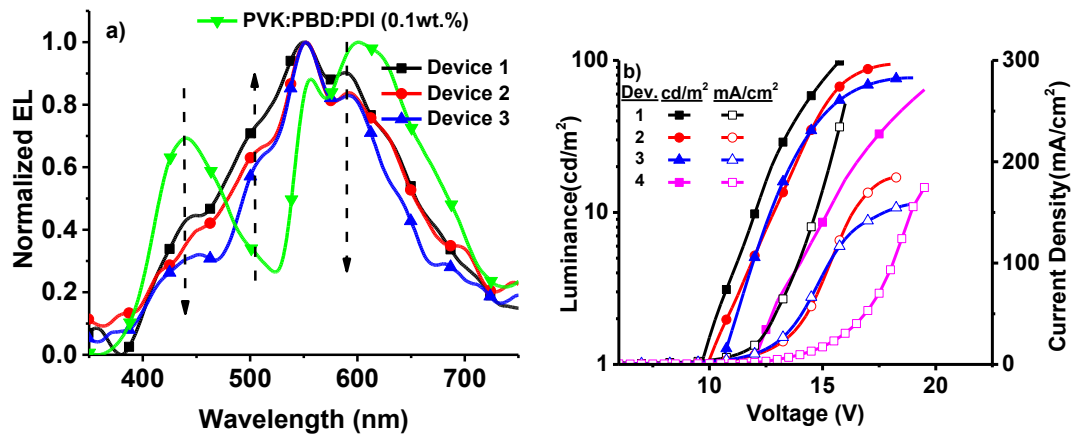
Figure 3.12. a) Normalized EL curves of Device 1-3 in comparison with normalized EL curve of bare PDI device and b) luminance-V-current density characteristics of Device1-3.

Table 3.3. CRI, CCT and CIE values Device 1-4 @ maximum brightness

Device #	CRI	CCT	CIE
1	92	3790	0.37, 0.35
2	90	3773	0.37, 0.36
3	84	4634	0.36, 0.36
4	96	4916	0.34, 0.36

The white light properties of Device 1-3 are given in Table 2. Combination of blue, green and orange-red emitter resulted in a CRI value higher than 90. However, white light characteristic is reduced from Device 1 to Device 3. By considering the discussions provided above, in order to regain the green photons absorbed by PDI and increase the

host concentration in emitting layer, reducing the PDI wt% is employed. Device 4 with an emitting layer of PVK:PBD: 0.06 wt% PDI: 0.03 wt% PTE is prepared. Its EL spectrum presented a full visible range coverage (Figure 3.13) with the combination of dominated peaks at 445, 535, 620 nm. These peak points are attributed to the EL of PVK:PBD, addition of emitted photons of host:PTE electroplex, PTE and PDI EL, and host:PDI exciplex and PDI, respectively. White light properties of 96 CRI, 4916 K CCT and (0.34, 0.36) CIE coordinates are achieved.
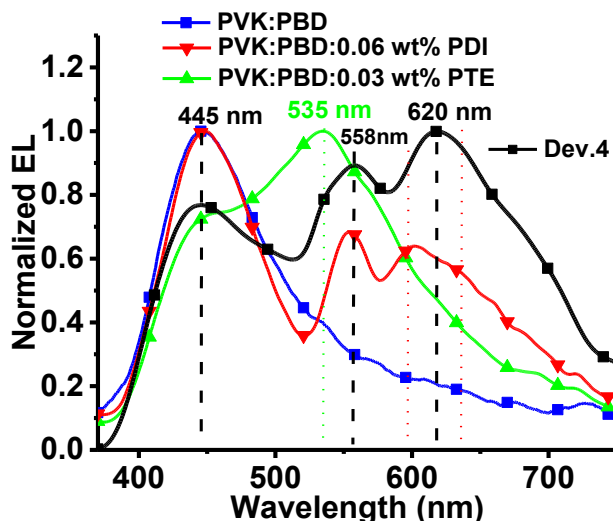
Figure 3.13. Normalized EL spectrum of Device 4 (dev.4, black) in comparison with the normalized EL spectra of PVK:PBD (blue), PVK:PBD:(0.03%)PTE (green) and PVK:PBD:(0.06%)PDI (red) emitting devices (EQE, current efficiency and Power efficiency in Appendix C).

In voltage-dependent EL measurements, it is seen that the green region becomes dominant with increasing voltage (figure 3.14). There was a reduction in both the blue emission from the host and the red emission from the PDI. 96 CRI value was obtained at 19V in device 4 with triple colour study (R, G, B) performed to achieve perfect color harmony. Lethal time measurements result of devices 1-4 are given figure 3.14 and device4 exhibited the longest lethal time (for LT70) compared to device 1-3. Blue, green and red colour intensities have been optimized at 19 V, resulted CRI value of 96.

There is only one WOLED study using perylene derivative [48]. Instead of coating ETL with vacuum thermal evaporation, in this study a simpler device structure has been achieved by blending electron transfer materials and hole transfer material as a host. In addition, this study is the first WOLED study using three primary colours. The highest CRI value obtained in the perylene WOLED literature was achieved due to the use of

three primary colours were also taken for the first time for perylene diimide derivatives-based OLED.
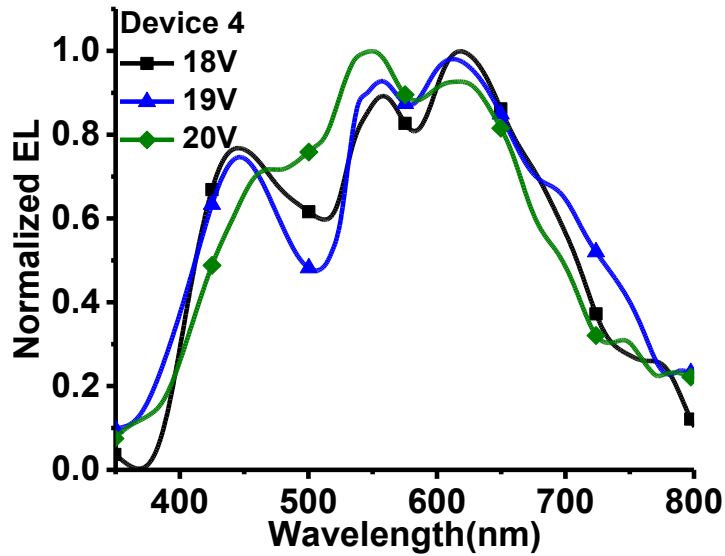

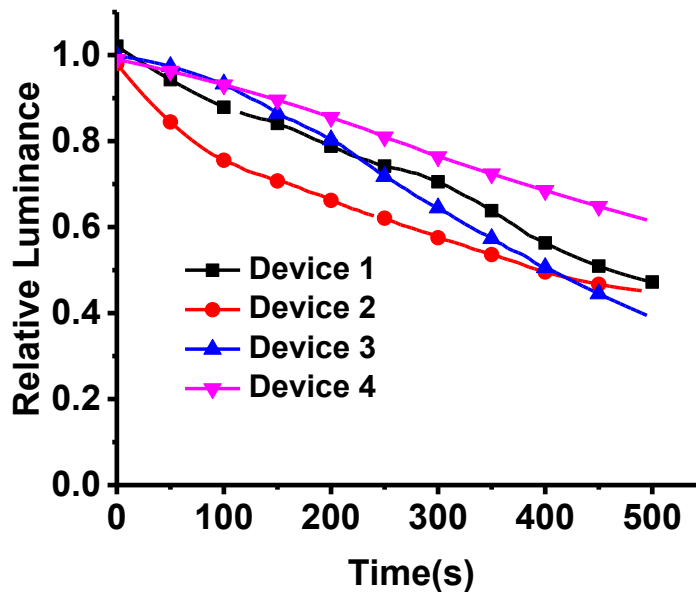Figure 3.14. EL spectrum of Device 4 under different potential (at 18, 19 and 20V)

Figure 3.15. Lethal time(LT70) of device 1-4 (with error bar see Appendix D)

Finally, the lethal times of the optimized devices were examined. In devices 1-3, the green zone dominated the radiation observed and these devices have degraded more quickly compared to device 4. In Device 1-3 emission is dominated from PTE (green zone) the fact that all radiation is on a single molecule may have negatively affected the life time of device. When the radiation is obtained from all materials homogeneously, it has been observed that it has both high CRI value and long-life time.

CONCLUSION

In summary, starting from the host choice and optimization of the dopant ratios, a perylene based solution processed single layer WOLED with white light properties of 96 CRI, 4916 K CCT and (0.34, 0.36) CIE coordinates are introduced. To the best of our knowledge, these values represent the best of current solution processed perylene based WOLED literature. Comparison of PL and EL spectra of the films and devices, respectively addressed that the orange-red emission was dominated by the exciplex formation whereas green emission was mainly generated from the electroplex emission. Energy transfer from the host to the green emitting PTE is more efficient than that of to the orange-red emitting PDI, but the lack of the red region resulted in CRI values of only around 75 in bare PTE devices. The highest CRI value obtained with bare PDI devices was 90.

REFERENCES

(1) International Year of Light and Light-Based Technologies. *https://www.light2015.org/Home/ScienceStories/Discoverers-of-Light--.html* **2015**, No. 08.11.2020.

(2) Https://Www.Light2015.Org/. *https://www.light2015.org/* **2015**, No. 08.11.2020.

(3) Gather, M. C.; Köhnen, A.; Meerholz, K. White Organic Light-Emitting Diodes. *Adv. Mater.* **2011**, *23* (2), 233–248. https://doi.org/10.1002/adma.201002636.

(4) Dr Khasha Ghaffarzadeh and Dr Norman Bardsley. OLED Lighting Opportunities 2017-2027: Forecasts, Technologies, Players.

(5) Https://Www.Lg.Com/Us/Tvs/Lg-Oled65wxpua-Oled-4k-Tv#.

(6) D'Andrade, B. W.; Esler, J.; Lin, C.; Adamovich, V.; Xia, S.; Weaver, M. S.; Kwong, R.; Brown, J. J. Realizing White Phosphorescent 100 Lm/W OLED Efficacy. *Org. Light Emit. Mater. Devices XII* **2008**, *7051*, 70510Q. https://doi.org/10.1117/12.793758.

(7) Barbrow, L. E. International Lighting Vocabulary. *J. SMPTE* **2012**. https://doi.org/10.5594/j07262.

(8) SONG, D. W. ORGANIC LIGHT-EMITTING DIODES AND RELATED HYBRID LIGHT-EMITTING DEVICES. **2011**.

(9) Lossev, O. V. CII. Luminous Carborundum Detector and Detection Effect and Oscillations with Crystals . *London, Edinburgh, Dublin Philos. Mag. J. Sci.* **1928**, *6* (39), 1024–1044. https://doi.org/10.1080/14786441108564683.

(10) Pope, M.; Kallmann, H. P.; Magnante, P. Electroluminescence in Organic Crystals [16]. *J. Chem. Phys.* **1963**, *38* (8), 2042–2043. https://doi.org/10.1063/1.1733929.

(11) Tang, C. W. W.; Vanslyke, S. A. A. Organic Electroluminescent Diodes. *Appl. Phys. Lett.* **1987**, *51* (12), 913–915. https://doi.org/10.1063/1.98799.

(12) Kido, J.; Hongawa, K.; Okuyama, K.; Nagai, K. White Light-Emitting Organic Electroluminescent Devices Using the Poly(N-Vinylcarbazole) Emitter Layer Doped with Three Fluorescent Dyes. *Appl. Phys. Lett.* **1994**, *64* (7), 815–817. https://doi.org/10.1063/1.111023.

(13) Adamovich, V.; Brooks, J.; Tamayo, A.; Alexander, A. M.; Djurovich, P. I.; D'Andrade, B. W.; Adachi, C.; Forrest, S. R.; Thompson, M. E. High Efficiency Single Dopant White Electrophosphorescent Light Emitting Diodesy. *New J.*

Chem. **2002**, *26* (9), 1171–1178. https://doi.org/10.1039/b204301g.

(14)   Sun, Y.; Forrest, S. R. Enhanced Light Out-Coupling of Organic Light-Emitting Devices Using Embedded Low-Index Grids. *Nat. Photonics* **2008**, *2* (8), 483–487. https://doi.org/10.1038/nphoton.2008.132.

(15)   Reineke, S.; Lindner, F.; Schwartz, G.; Seidler, N.; Walzer, K.; Lüssem, B.; Leo, K. White Organic Light-Emitting Diodes with Fluorescent Tube Efficiency. *Nature* **2009**, *459* (7244), 234–238. https://doi.org/10.1038/nature08003.

(16)   http://www.oled.at/. Http://Www.Oled.at/Osram-Zeigt-Neue-Technologie-Fuer-Grosse-Transparente-Oleds/. **2009**, No. access date 07.11.2020.

(17)   OLLA Projet Oled-Info. *https://www.oled-info.com/lifetime/olla_oled_project_extends_white_light_potential*.

(18)   OLED100.Eu. *https://www.oled-info.com/oled100eu*.

(19)   Https://Www.Oled-Info.Com/Soledlight.

(20)   Sadig Aghazada, Aron J. Huckaba, Antonio Pertegas, Azin Babaei, Giulia Grancini, Iwan Zimmermann, Henk Bolink, M. K. N. Molecular Engineering of Iridium Blue Emitters Using Aryl N- Heterocyclic Carbene Ligands. *Eur. J. Inorg. Chem.* **2016**, No. 32, 5089–5097.

(21)   Mladenovski, S.; Neyts, K.; Pavicic, D.; Werner, A.; Rothe, C. Exceptionally Efficient Organic Light Emitting Devices Using High Refractive Index Substrates. *Opt. Express* **2009**, *17* (9), 7562. https://doi.org/10.1364/oe.17.007562.

(22)   Kanno, H.; Holmes, R. J.; Sun, Y.; Kena-Cohen, S.; Forrest, S. R. White Stacked Electrophosphorescent Organic Light-Emitting Devices Employing MoO3 as a Charge-Generation Layer. *Adv. Mater.* **2006**, *18* (3), 339–342. https://doi.org/10.1002/adma.200501915.

(23)   Hua, W.; Du, X.; Su, W.; Lin, W.; Zhang, D. Full Phosphorescent White-Light Organic Light-Emitting Diodes with Improved Color Stability and Efficiency by Fine Tuning Primary Emission Contributions. *AIP Adv.* **2014**, *4* (2). https://doi.org/10.1063/1.4865209.

(24)   D'Andrade, B. W.; Thompson, M. E.; Forrest, S. R. Controlling Exciton Diffusion in Multilayer White Phosphorescent Organic Light Emitting Devices. *Adv. Mater.* **2002**, *14* (2), 147–151. https://doi.org/10.1002/1521-4095(20020116)14:2<147::AID-ADMA147>3.0.CO;2-3

(25)   Tokito, S.; Iijima, T.; Tsuzuki, T.; Sato, F. High-Efficiency White Phosphorescent Organic Light-Emitting Devices with Greenish-Blue and Red-Emitting Layers.

Appl. Phys. Lett. **2003**, *83* (12), 2459–2461. https://doi.org/10.1063/1.1611620.

(26) Kim, C. H.; Shinar, J. Bright Small Molecular White Organic Light-Emitting Devices with Two Emission Zones. *Appl. Phys. Lett.* **2002**, *80* (12), 2201–2203. https://doi.org/10.1063/1.1464223.

(27) Alam, M. M.; Jenekhe, S. A. Binary Blends of Polymer Semiconductors: Nanocrystalline Morphology Retards Energy Transfer and Facilitates Efficient White Electroluminescence. *Macromol. Rapid Commun.* **2006**, *27* (24), 2053–2059. https://doi.org/10.1002/marc.200600603.

(28) Wu, Z.; Ma, D. Recent Advances in White Organic Light-Emitting Diodes. **2016**, *107*, 1–42.

(29) Shirakawa, H.; Louis, E. J.; MacDiarmid, A. G.; Chiang, C. K.; Heeger, A. J. Synthesis of Electrically Conducting Organic Polymers: Halogen Derivatives of Polyacetylene, (CH)X. *J. Chem. Soc. Chem. Commun.* **1977**, No. 16, 578–580. https://doi.org/10.1039/C39770000578.

(30) Audenaert, M.; Gusman, G.; Deltour, R. Electrical Conductivity of I2-Doped Polyacetylene. *Phys. Rev. B* **1981**, *24* (12), 7380–7382. https://doi.org/10.1103/PhysRevB.24.7380.

(31) Adachi, C.; Baldo, M. A.; Thompson, M. E.; Forrest, S. R. Nearly 100% Internal Phosphorescence Efficiency in an Organic Light Emitting Device. *J. Appl. Phys.* **2001**, *90* (10), 5048–5051. https://doi.org/10.1063/1.1409582.

(32) Chiang, C. J.; Kimyonok, A.; Etherington, M. K.; Griffiths, G. C.; Jankus, V.; Turksoy, F.; Monkman, A. P. Ultrahigh Efficiency Fluorescent Single and Bi-Layer Organic Light Emitting Diodes: The Key Role of Triplet Fusion. *Adv. Funct. Mater.* **2013**, *23* (6), 739–746. https://doi.org/10.1002/adfm.201201750.

(33) Siboni, H. Z.; Aziz, H. Triplet-Polaron Quenching by Charges on Guest Molecules in Phosphorescent Organic Light Emitting Devices. *Appl. Phys. Lett.* **2012**, *101* (6). https://doi.org/10.1063/1.4745194.

(34) Sato, K.; Shizu, K.; Yoshimura, K.; Kawada, A.; Miyazaki, H.; Adachi, C. Organic Luminescent Molecule with Energetically Equivalent Singlet and Triplet Excited States for Organic Light-Emitting Diodes. *Phys. Rev. Lett.* **2013**, *110* (24), 1–5. https://doi.org/10.1103/PhysRevLett.110.247401.

(35) Reineke, S.; Walzer, K.; Leo, K. Triplet-Exciton Quenching in Organic Phosphorescent Light-Emitting Diodes with Ir-Based Emitters. *Phys. Rev. B - Condens. Matter Mater. Phys.* **2007**, *75* (12), 1–13.

https://doi.org/10.1103/PhysRevB.75.125328.

(36) Forrest, S. R.; O'Brien, D. F. Excitonic Singlet-Triplet Ratio in a Semiconducting Organic Thin Film. *Phys. Rev. B - Condens. Matter Mater. Phys.* **1999**, *60* (20), 14422–14428. https://doi.org/10.1103/PhysRevB.60.14422.

(37) Li, J.; Nakagawa, T.; Macdonald, J.; Zhang, Q.; Nomura, H.; Miyazaki, H.; Adachi, C. Highly Efficient Organic Light-Emitting Diode Based on a Hidden Thermally Activated Delayed Fluorescence Channel in a Heptazine Derivative. *Adv. Mater.* **2013**, *25* (24), 3319–3323. https://doi.org/10.1002/adma.201300575.

(38) Tanaka, H.; Shizu, K.; Miyazaki, H.; Adachi, C. Efficient Green Thermally Activated Delayed Fluorescence (TADF) from a Phenoxazine–Triphenyltriazine (PXZ–TRZ) Derivative. *Chem. Commun.* **2012**, *48* (93), 11392–11394. https://doi.org/10.1039/c2cc36237f.

(39) Reineke, S. Controlling Excitons - Concepts for Phosphorscent Organic LEDs at High Brightness. **2009**, No. PhD thesis.

(40) Nakayama, K.; Hirose, Y.; Soeda, J.; Yoshizumi, M.; Uemura, T.; Uno, M.; Li, W.; Kang, M. J.; Yamagishi, M.; Okada, Y.; Miyazaki, E.; Nakazawa, Y.; Nakao, A.; Takimiya, K.; Takeya, J. Patternable Solution-Crystallized Organic Transistors with High Charge Carrier Mobility. *Adv. Mater.* **2011**, *23* (14), 1626–1629. https://doi.org/10.1002/adma.201004387.

(41) Chu, T. Y.; Song, O. K. Hole Mobility of N, N′ -Bis(Naphthalen-1-Yl)- N, N′ - Bis(Phenyl) Benzidine Investigated by Using Space-Charge-Limited Currents. *Appl. Phys. Lett.* **2007**, *90* (20), 1–4. https://doi.org/10.1063/1.2741055.

(42) Aksoy, E.; Demir, N.; Varlikli, C. White LED Light Production by Using Dibromoperylene Derivatives in down Conversion of Energy. *Can. J. Phys.* **2018**, *96*, 734–739. https://doi.org/https://doi.org/10.1139/cjp-2017-0752.

(43) Chang, H.; Chen, Z.; Yang, X.; Yin, Q.; Zhang, J.; Ying, L.; Jiang, X. F.; Xu, B.; Huang, F.; Cao, Y. Novel Perylene Diimide Based Polymeric Electron-Acceptors Containing Ethynyl as the π-Bridge for All-Polymer Solar Cells. *Org. Electron.* **2017**, *45*, 227–233. https://doi.org/10.1016/j.orgel.2017.03.022.

(44) Zhang, B.; Soleimaninejad, H.; Jones, D. J.; White, J. M.; Ghiggino, K. P.; Smith, T. a.; Wong, W. W. H. Highly Fluorescent Molecularly Insulated Perylene Diimides: Effect of Concentration on Photophysical Properties. *Chem. Mater.* **2017**, *29* (19), 8395–8403. https://doi.org/10.1021/acs.chemmater.7b02968.

(45) Lin, Y.; Zhan, X. Designing Efficient Non-Fullerene Acceptors by Tailoring

Extended Fused-Rings with Electron-Deficient Groups. *Adv. Energy Mater.* **2015**, *5* (20), 1–9. https://doi.org/10.1002/aenm.201501063.

(46)   Matussek, M.; Filapek, M.; Gancarz, P.; Krompiec, S.; Grzegorz Małecki, J.; Kotowicz, S.; Siwy, M.; Maćkowski, S.; Chrobok, A.; Schab-Balcerzak, E.; Słodek, A. Synthesis and Photophysical Properties of New Perylene Bisimide Derivatives for Application as Emitting Materials in OLEDs. *Dye. Pigment.* **2018**, *159* (June), 590–599. https://doi.org/10.1016/j.dyepig.2018.07.006.

(47)   Zong, L.; Gong, Y.; Yu, Y.; Xie, Y.; Xie, G.; Peng, Q.; Li, Q.; Li, Z. New Perylene Diimide Derivatives: Stable Red Emission, Adjustable Property from ACQ to AIE, and Good Device Performance with an EQE Value of 4.93%. *Sci. Bull.* **2018**, *63* (2), 108–116. https://doi.org/10.1016/j.scib.2017.10.021.

(48)   Gupta, R. K.; Das, D.; Iyer, P. K.; Achalkumar, A. S. First Example of White Organic Electroluminescence Utilizing Perylene Ester Imides. *ChemistrySelect* **2018**, *3* (18), 5123–5129. https://doi.org/10.1002/slct.201801258.

(49)   Gupta, R. K.; Ulla, H.; Satyanarayan, M. N.; Sudhakar, A. A. A Perylene-Triazine-Based Star-Shaped Green Light Emitter for Organic Light Emitting Diodes. *European J. Org. Chem.* **2018**, *2018* (13), 1608–1613. https://doi.org/10.1002/ejoc.201800161.

(50)   Gupta, R. K.; Das, D.; Gupta, M.; Pal, S. K.; Iyer, P. K.; Achalkumar, A. S. Electroluminescent Room Temperature Columnar Liquid Crystals Based on Bay-Annulated Perylene Tetraesters. *J. Mater. Chem. C* **2017**, *5* (7), 1767–1781. https://doi.org/10.1039/c6tc04166c.

(51)   Kozma, E.; Mróz, W.; Villafiorita-Monteleone, F.; Galeotti, F.; Andicsová-Eckstein, A.; Catellani, M.; Botta, C. Perylene Diimide Derivatives as Red and Deep Red-Emitters for Fully Solution Processable OLEDs. *RSC Adv.* **2016**, *6* (66), 61175–61179. https://doi.org/10.1039/c6ra10467c.

(52)   Li, G.; Zhao, Y.; Li, J.; Cao, J.; Zhu, J.; Sun, X. W.; Zhang, Q. Synthesis, Characterization, Physical Properties, and OLED Application of Single BN-Fused Perylene Diimide. *J. Org. Chem.* **2015**, *80* (1), 196–203. https://doi.org/10.1021/jo502296z.

(53)   Oner, I.; Varlikli, C.; Icli, S. The Use of a Perylenediimide Derivative as a Dopant in Hole Transport Layer of an Organic Light Emitting Device. *Appl. Surf. Sci.* **2011**, *257* (14), 6089–6094. https://doi.org/10.1016/j.apsusc.2011.02.002.

(54)   Céspedes-Guirao, F. J.; García-Santamaría, S.; Fernndez-Lzaro, F.; Sastre-Santos,

A.; Bolink, H. J. Efficient Electroluminescence from a Perylenediimide Fluorophore Obtained from a Simple Solution Processed OLED. *J. Phys. D. Appl. Phys.* **2009**, *42* (10). https://doi.org/10.1088/0022-3727/42/10/105106.

(55) Dyad, P.; Costa, R. D.; Céspedes-guirao, F. J.; Ortí, E.; Bolink, H. J. Efficient Deep-Red Light-Emitting Electrochemical Cells Based on A. **2009**, No. c, 1–13.

(56) Del Cano, T.; Hashimoto, K.; Kageyama, H.; De Saja, J. A.; Aroca, R.; Ohmori, Y.; Shirota, Y. Near-Infrared Electroluminescence Based on Perylenediimide-Doped Tris(8-Quinolinolato) Aluminum. *Appl. Phys. Lett.* **2006**, *88* (7), 78–81. https://doi.org/10.1063/1.2170427.

(57) Kumar, M.; Pereira, L. Towards Highly Efficient TADF Yellow-Red OLEDs Fabricated by Solution Deposition Methods: Critical Influence of the Active Layer Morphology. *Nanomaterials* **2020**, *10* (1). https://doi.org/10.3390/nano10010101.

(58) Yap, C. C.; Yahaya, M.; Salleh, M. M. The Effect of DCJTB Concentration on the Photoluminescent and Electroluminescent Properties of PVK–PBD–Perylene–DCJTB Thin Films. *Mater. Sci. Pol.* **2009**, *27* (January 2009), 1.

(59) Yap, C. C.; Yahaya, M.; Salleh, M. M. Influence of Thickness of Functional Layer on Performance of Organic Salt-Doped OLED with ITO/PVK:PBD:TBAPF6/Al Structure. *Curr. Appl. Phys.* **2008**, *8* (5), 637–644. https://doi.org/10.1016/j.cap.2007.11.006.

(60) Jiang, X.; Register, R. A.; Killeen, K. A.; Thompson, M. E.; Pschenitzka, F.; Hebner, T. R.; Sturm, J. C. Effect of Carbazole-Oxadiazole Excited-State Complexes on the Efficiency of Dye-Doped Light-Emitting Diodes. *J. Appl. Phys.* **2002**, *91* (10 I), 6717–6724. https://doi.org/10.1063/1.1469692.

(61) Zhong, P. L.; Zheng, C. J.; Zhang, M.; Zhao, J. W.; Yang, H. Y.; He, Z. Y.; Lin, H.; Tao, S. L.; Zhang, X. H. Highly Efficient Ternary Polymer-Based Solution-Processable Exciplex with over 20% External Quantum Efficiency in Organic Light-Emitting Diode. *Org. Electron.* **2020**, *76* (August 2019), 1–7. https://doi.org/10.1016/j.orgel.2019.105449.

(62) Kumar, M.; Pereira, L. Mixed-Host Systems with a Simple Device Structure for Efficient Solution-Processed Organic Light-Emitting Diodes of a Red-Orange TADF Emitter. *ACS Omega* **2020**, *5* (5), 2196–2204. https://doi.org/10.1021/acsomega.9b03253.

(63) Li, N.; Zhang, Y.; Quan, Y.; Li, L.; Ye, S.; Fan, Q.; Huang, W. High-Efficiency Solution-Processed WOLEDs with Very High Color Rendering Index Based on a
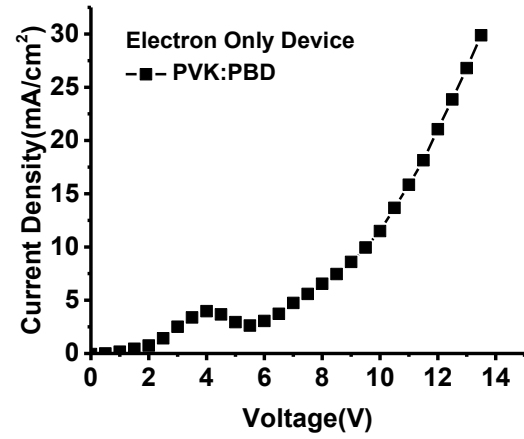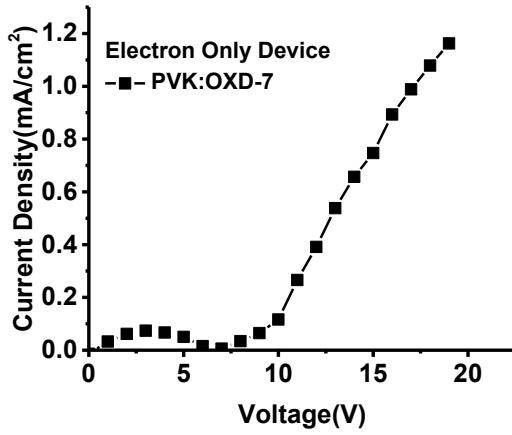
Macrospirocyclic Oligomer Matrix Host. *Opt. Mater. Express* **2018**, *8* (10), 3208. https://doi.org/10.1364/ome.8.003208.

(64)   Song, W.; Lee, J. Y.; Cho, Y. J.; Yu, H.; Aziz, H.; Lee, K. M. Electroplex as a New Concept of Universal Host for Improved Efficiency and Lifetime in Red, Yellow, Green, and Blue Phosphorescent Organic Light-Emitting Diodes. *Adv. Sci.* **2018**, *5* (2). https://doi.org/10.1002/advs.201700608.

(65)   Guner, T.; Aksoy, E.; Demir, M. M.; Varlikli, C. Perylene-Embedded Electrospun PS Fibers for White Light Generation. *Dye. Pigment.* **2019**, *160* (August 2018), 501–508. https://doi.org/10.1016/j.dyepig.2018.08.040.

(66)   Aksoy, E. Organik Fotonik Sistemlerde Kullanilabilecek Perilendiimit Türevlerinin Sentezi ve Fotofiziksel Karakterizasyonu. **2020**.

(67)   Zhang, C.; von Seggern, H.; Pakbaz, K.; Kraabel, B.; Schmidt, H. W.; Heeger, A. J. Blue Electroluminescent Diodes Utilizing Blends of Poly(p-Phenylphenylene Vinylene) in Poly(9-Vinylcarbazole). *Synth. Met.* **1994**, *62* (1), 35–40. https://doi.org/10.1016/0379-6779(94)90196-1.

(68)   Chihaya Adachi, Tetsuo Tsutsui, and S. S. Organic Electroluminescent Device Having a Hole Conductor as an Emitting Layer. **1989**, *55*, 1489.

(69)   Hamada, Y.; Adachi, C.; Tsutsui, T.; Saito, S. Blue-Light-Emitting Organic Electroluminescent Devices with Oxadiazole Dimer Dyes as an Emitter. *Jpn. J. Appl. Phys.* **1992**, *31* (6 R), 1812–1816. https://doi.org/10.1143/JJAP.31.1812.

(70)   Chang, Y. T.; Chang, J. K.; Lee, Y. T.; Wang, P. S.; Wu, J. L.; Hsu, C. C.; Wu, I. W.; Tseng, W. H.; Pi, T. W.; Chen, C. T.; Wu, C. I. High-Efficiency Small-Molecule-Based Organic Light Emitting Devices with Solution Processes and Oxadiazole-Based Electron Transport Materials. *ACS Appl. Mater. Interfaces* **2013**, *5* (21), 10614–10622. https://doi.org/10.1021/am402504g.

(71)   Yang, X.; Wu, F. I.; Haverinen, H.; Li, J.; Cheng, C. H.; Jabbour, G. E. Efficient Organic Light-Emitting Devices with Platinum-Complex Emissive Layer. *Appl. Phys. Lett.* **2011**, *98* (3). https://doi.org/10.1063/1.3541447.

(72)   Das, D.; Gopikrishna, P.; Narasimhan, R.; Singh, A.; Dey, A.; Iyer, P. K. White Polymer Light Emitting Diodes Based on PVK: The Effect of the Electron Injection Barrier on Transport Properties, Electroluminescence and Controlling the Electroplex Formation. *Phys. Chem. Chem. Phys.* **2016**, *18* (48), 33077–33084. https://doi.org/10.1039/c6cp07092b.

(73)   Mott, N. F. *Electronic Processes in Ionic Crystals*; Oxford University Press, 1940.

(74) Ho, C. L.; Wong, W. Y.; Zhou, G. J.; Yao, B.; Xie, Z.; Wang, L. Solution-Processible Multi-Component Cyclometalated Iridium Phosphors for High-Efficiency Orange-Emitting OLEDs and Their Potential Use as White Light Sources. *Adv. Funct. Mater.* **2007**, *17* (15), 2925–2936. https://doi.org/10.1002/adfm.200601205.

(75) Höfle, S.; Lutz, T.; Egel, A.; Nickel, F.; Kettlitz, S. W.; Gomard, G.; Lemmer, U.; Colsmann, A. Influence of the Emission Layer Thickness on the Optoelectronic Properties of Solution Processed Organic Light-Emitting Diodes. *ACS Photonics* **2014**, *1* (10), 968–973. https://doi.org/10.1021/ph500186m.

(76) Agrawal, R.; Kumar, P.; Ghosh, S.; Mahapatro, A. K. Thickness Dependence of Space Charge Limited Current and Injection Limited Current in Organic Molecular Semiconductors. *Appl. Phys. Lett.* **2008**, *93* (7). https://doi.org/10.1063/1.2974084.

(77) Jayaram, B.; Singh, T.; Mukherjee, G.; Mathur, A.; Shekhar, S.; Shekhar, V. Sanjeevini: A Freely Accessible Web-Server for Target Directed Lead Molecule Discovery. *BMC Bioinformatics* **2012**, *13 Suppl 1* (Suppl 17). https://doi.org/10.1186/1471-2105-13-S17-S7.

(78) Yokoyama, D. Molecular Orientation in Small-Molecule Organic Light-Emitting Diodes. *J. Mater. Chem.* **2011**, *21* (48), 19187–19202. https://doi.org/10.1039/c1jm13417e.

(79) Friederich, P.; Rodin, V.; Von Wrochem, F.; Wenzel, W. Built-In Potentials Induced by Molecular Order in Amorphous Organic Thin Films. *ACS Appl. Mater. Interfaces* **2018**, *10* (2), 1881–1887. https://doi.org/10.1021/acsami.7b11762.

(80) Wen, L.; Li, F.; Xie, J.; Wu, C.; Zheng, Y.; Chen, D.; Xu, S.; Guo, T.; Qu, B.; Chen, Z.; Gong, Q. Electroplex Emission at PVK/Bphen Interface for Application in White Organic Light-Emitting Diodes. *J. Lumin.* **2011**, *131* (11), 2252–2254. https://doi.org/10.1016/j.jlumin.2011.05.056.

(81) Zhao, D. W.; Xu, Z.; Zhang, F. J.; Song, S. F.; Zhao, S. L.; Wang, Y.; Yuan, G. C.; Zhang, Y. F.; Xu, H. H. The Effect of Electric Field Strength on Electroplex Emission at the Interface of NPB/PBD Organic Light-Emitting Diodes. *Appl. Surf. Sci.* **2007**, *253* (8), 4025–4028. https://doi.org/10.1016/j.apsusc.2006.08.046.

(82) Hao, Y.; Meng, W.; Xu, H.; Wang, H.; Liu, X.; Xu, B. White Organic Light-Emitting Diodes Based on a Novel Zn Complex with High CRI Combining Emission from Excitons and Interface-Formed Electroplex. *Org. Electron.* **2011**, *12* (1), 136–142. https://doi.org/10.1016/j.orgel.2010.10.019.

(83)   Zeng, H.; Huang, Q.; Liu, J.; Huang, Y.; Zhou, J.; Zhao, S.; Lu, Z. A Red-Emissive Sextuple Hydrogen-Bonding Self-Assembly Molecular Duplex Bearing Perylene Diimide Fluorophores for Warm-White Organic Light-Emitting Diode Application. *Chinese J. Chem.* **2016**, *34* (4), 387–396. https://doi.org/10.1002/cjoc.201500771.
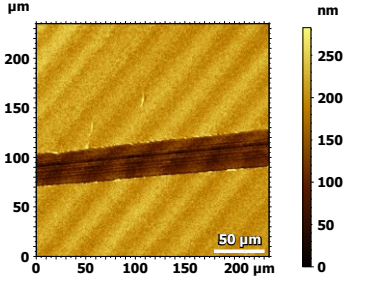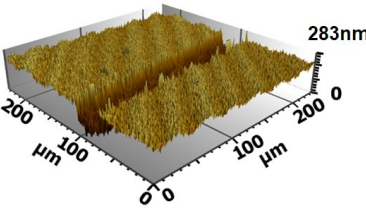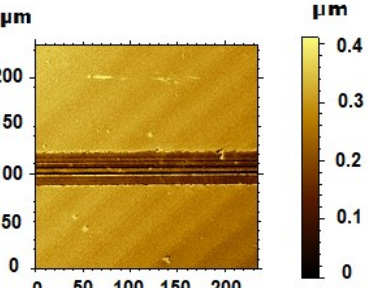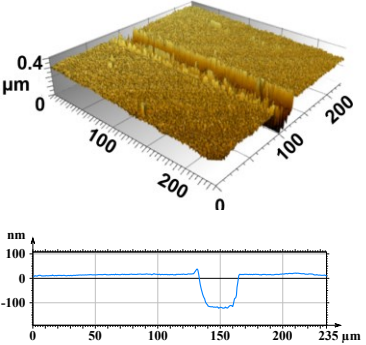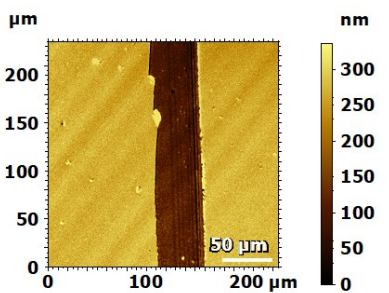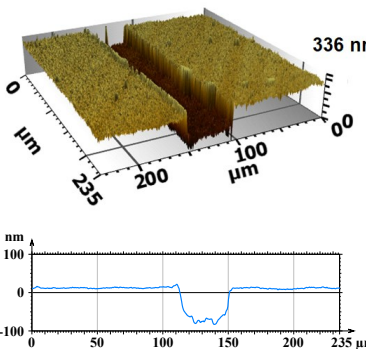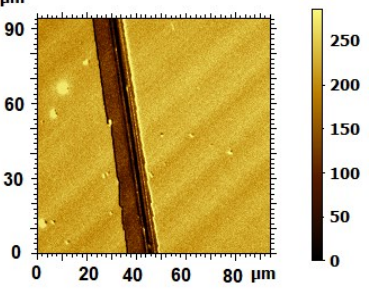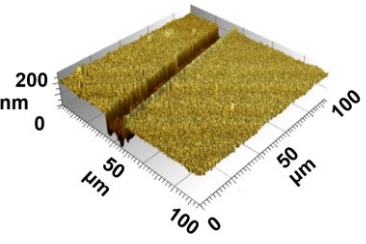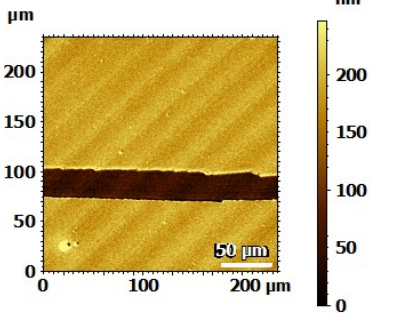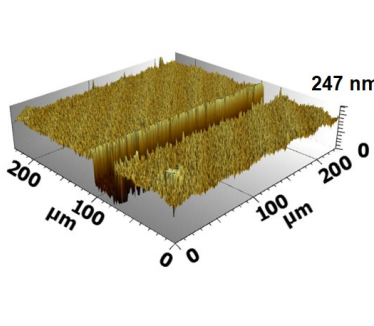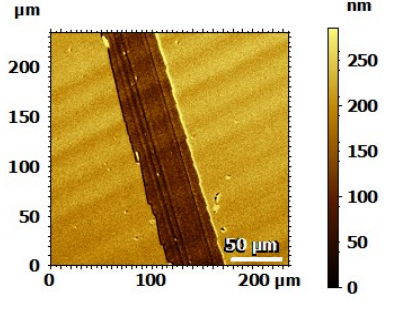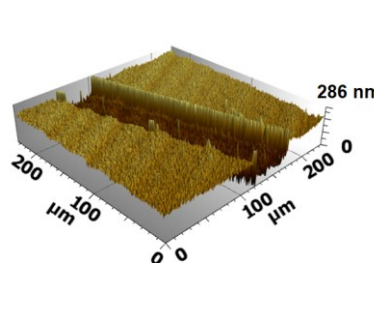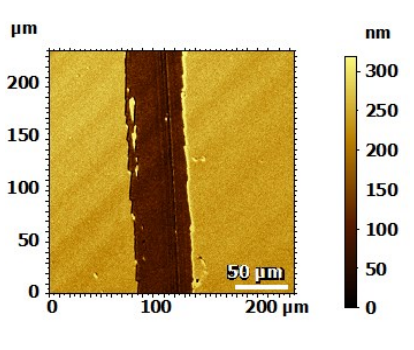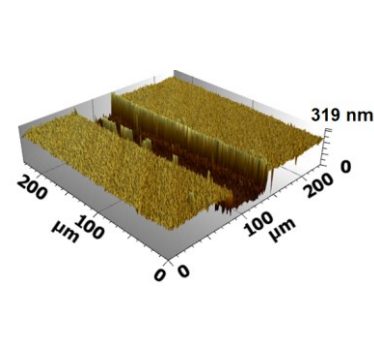
APPENDIX A

Current density-Voltage characteristic of electron and hole only device of PVK:PBD and PVK:OXD-7
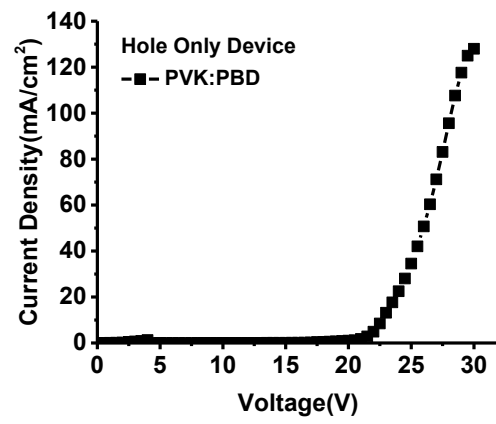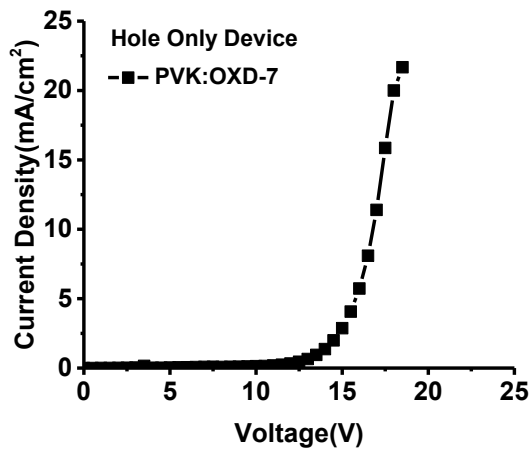
APPENDIX B

Thickness measurements of layers

Active layer	2D	3D	Avg. Thick.
PEDOT:PSS			75±3.2 nm
PVK: OXD7			126±4.3 nm
PVK: PBD			84±2.0 nm
PVK: OXD-7: PDI (0.1 wt%)			135±4.9 nm

Active layer	2D	3D	Avg. Thick.
PVK: PBD: PDI (0.1 wt%)			89±3.4 nm
PVK: PBD: PTE (0.1 wt%)			87±2.8 nm
PVK: PBD: PDI (0.1 wt%): PTE (0.1 wt%)			87±2.1 nm

APPENDIX C

a) EQE, b) Current efficiency and c) Power efficiency of Device1-4
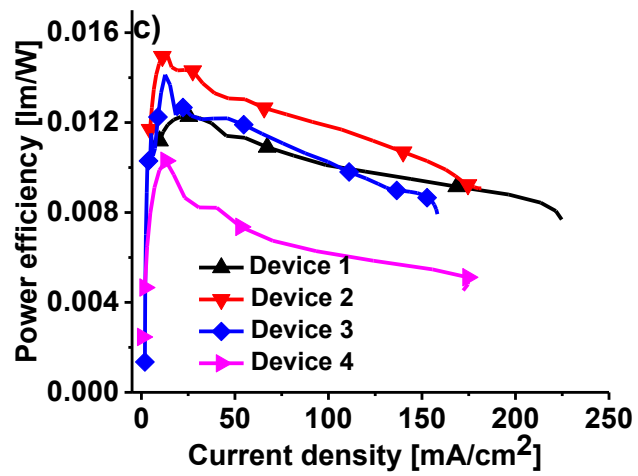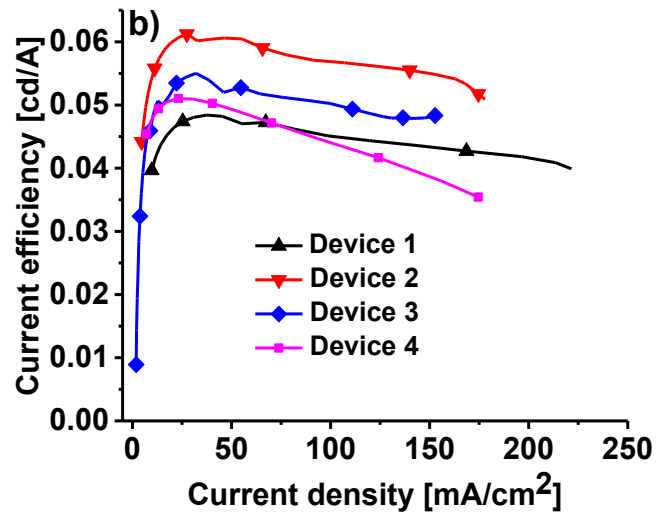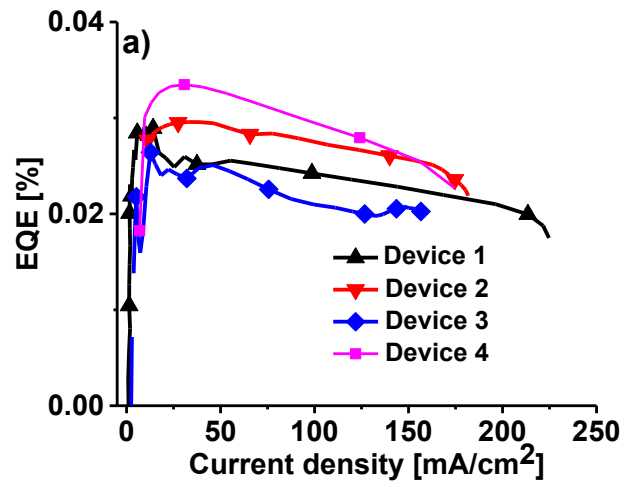
APPENDIX D

Lethal time of a) Device 1 b) Device 2 c) Device 3 d) Device 4